ANL/OEPM-80-17

ANL/OEPM-80-17

ANNUAL REPORT FOR 1980 ON RESEARCH, DEVELOPMENT, AND DEMONSTRATION OF NICKEL-IRON BATTERIES FOR ELECTRIC VEHICLE PROPULSION

Contract No. 31-109-38-4141

by

Westinghouse Electric Corporation

ARGONNE NATIONAL LABORATORY

ARGONNE NATIONAL LABORATORY, ARGONNE, ILLINOIS

Operated for the U. S. DEPARTMENT OF ENERGY
under Contract W-31-109-Eng-38

DISCLAIMER

The facilities of Argonne National Laboratory are owned by the United States Government. Under the terms of a contract (W-31-109-Eng-38) among the U. S. Department of Energy, Argonne Universities Association and The University of Chicago, the University employs the staff and operates the Laboratory in accordance with policies and programs formulated, approved and reviewed by the Association.

MEMBERS OF ARGONNE UNIVERSITIES ASSOCIATION

The University of Arizona
Carnegie-Mellon University
Case Western Reserve University
The University of Chicago
University of Cincinnati
Illinois Institute of Technology
University of Illinois
Indiana University
The University of Iowa
Iowa State University
The University of Kansas
Kansas State University
Loyola University of Chicago
Marquette University
The University of Michigan
Michigan State University
University of Minnesota
University of Missouri
Northwestern University
University of Notre Dame
The Ohio State University
Ohio University
The Pennsylvania State University
Purdue University
Saint Louis University
Southern Illinois University
The University of Texas at Austin
Washington University
Wayne State University
The University of Wisconsin-Madison

Printed in the United States of America
Available from
National Technical Information Service
U. S. Department of Commerce
5285 Port Royal Road
Springfield, VA 22161

NTIS price codes
Printed copy: A06
Microfiche copy: A01

Distribution Category:
Energy Storage—Electrochemical--
Near-Term Batteries (UC-94ca)

ANL/OEPM-80-17

Annual Report for 1980 on

RESEARCH, DEVELOPMENT, AND DEMONSTRATION OF NICKEL-IRON BATTERIES FOR ELECTRIC VEHICLE PROPULSION

Prepared for

The Office for Electrochemical Project Management
Argonne National Laboratory
Under Contract No. 31-109-38-4141

by

Westinghouse Electric Corporation
Pittsburgh, Pennsylvania

March 1981

RESEARCH DEVELOPMENT, AND DEMONSTRATION OF A NICKEL/IRON BATTERY FOR ELECTRIC VEHICLE PROPULSION

R. Rosey, Program Manager
W. Feduska, Technical Coordinator

CONTRIBUTORS:

L. A. Doggrell, J. F. Jackovitz, C. W. Maiden
N. J. Maskalick, W. Pollack, L. C. Romain
J. Seidel, B. E. Taber

ANNUAL STATUS REPORT FOR FY '80
PUBLIC REPORT
CONTRACT NO. 31-109-38-4141

PREPARED FOR:

ARGONNE NATIONAL LABORATORY
Chemical Engineering Division
Office of Electrochemical Project Management
9700 South Cass Avenue
Argonne, Illinois 60439
N. P. YAO, Director
John Rajan, TASK LEADER

November 18, 1980

WESTINGHOUSE ELECTRIC CORPORATION
ADVANCED ENERGY SYSTEMS DIVISION
P. O. Box 10864
Pittsburgh, PA 15236

TABLE OF CONTENTS

TABLE OF CONTENTS (Continued)

TABLE OF CONTENTS (Continued)

LIST OF ILLUSTRATIONS

LIST OF TABLES

ABSTRACT

The FY '80 program continued to involve full-size, prototype cell, module and battery fabrication and evaluation, aimed at advancing the technical capabilities of the nickel-iron battery, while simultaneously reducing its potential cost in materials and process areas. Improved Electroprecipitation Process (EPP) nickel electrodes of design thickness (2.5 mm) are now being prepared that display stable capacities of 23 to 25 Ah for the C/3 drain rate at 200+ test cycles. Iron electrodes of the composite-type are delivering 24 Ah at the target thickness (1.0 mm). Iron electrodes are displaying capacity stability for >1000 test cycles in continuing 3 plate cell tests. Finished cells have delivered 57 to 61 Wh/kg at C/3, and have demonstrated cyclic stability to 500+ cycles at 80% depth of discharge profiles at Westinghouse. A 6-cell module that demonstrated 239 Ah, 1735 Wh, 48 Wh/kg at the C/3 drain rate has also been evaluated at the National Battery Test Laboratory (NBTL), Argonne National Laboratory. It operated for 327 test cycles, to a level of 161 Ah at the C/3 rate, before being removed from test.

Reduction in nickel electrode swelling (and concurrent stack starvation), to improve cycling, continues to be an area of major effort to reach the final battery cycle life objectives. Pasted nickel electrodes continue to show promise for meeting the life objectives while, simultaneously, providing a low manufacturing cost.

Refinements have occurred in the areas of cell hardware, module manifolding and cell interconnections as a result of a related DOE/JPL battery demonstration program. These improvements have been incorporated into the construction and testing of the cells and modules for this ANL/DOE program.

Temperature tests at 0°C have been performed on a 6-cell module and have shown a decrease in capacity of only 25% in ampere-hours and 29% in watt-hours as compared to 25°C performance. Additional tests are planned to demonstrate performance at -15°C and 40°C.

1.0 EXECUTIVE SUMMARY

The basic program objective is to accelerate the development of nickel-iron batteries and demonstrate improved performance features in electric vehicle battery systems. The Near term EV Battery Development goals based on the DOE/ETV-1 performance to be achieved by FY 1986 are:

56 Wh/kg	gravimetric energy density at C/3 rate
100 wh/l	volumetric energy density
104 w/kg	power density at 50% state of charge
800 cycles	life at 80% DOD cycles
70 $/kwh	1977 $ OEM selling price

The development approach was to utilize established Westinghouse technology that is capable of meeting the performance, life and cost objectives. The primary features of the Westinghouse design are the use of low cost raw materials, minimal use of nickel, and utilization of established manufacturing processes. A typical example is the use of sintered steel fiber electrode substrates that provide for a cell design with less than 50 percent the nickel content of other cells containing conventional sintered nickel electrodes.

Performance improvements achieved since initiation of contract. and demonstrated in cells and multi-cell modules at Westinghouse, include: 1) >30% increase in gravimetric energy density to 61 Wh/kg, 2) 70% increase in volumetric energy density to 120 Wh/l, and 3) a 5% increase in power density to 105 W/kg. In addition, a conceptual design has been established for a multi-cell modular package that can further enhance these performance parameters by providing additional 9% weight and 15% volume reductions.

The demonstrated performance at NBTL has indicated that an electric vehicle with characteristics similar to DOE ETV-1, with a Westinghouse nickel-iron battery, could attain a 100 mile range on the SAE J227a "D" cycle.

Several accomplishments have been made in process development by operating pilot line facilities to demonstrate the potential for $70/kwh OEM selling price. Cost reductions identified and incorporated in the pilot line production process include 1) demonstration of stitched steel fiber metal blanket manufacturing, 2) decreased cycle time and increased process efficiency for electroprecipitation process nickel electrodes, 3) activation techniques and paste manufacturing process for iron electrodes, and 4) identification of suitable separator systems.

Cycle life objectives remain to be demonstrated for modules and batteries. The potential for meeting the 800 cycle goal has been enhanced by demonstration of the following: 1) iron electrode life of >1,000 cycles at 80% DOD, 2) nickel electrode life of >1,000 cycles at 50% DOD, 3) cell life (220Ah) of >500 cycles @ 80% DOD, and 4) 5-cell module life of >325 cycles @ 80% DOD.

Several environmental issues have also been addressed in 1980. Low temperature performance of the battery has demonstrated that only a 25% decrease in capacity occurs for a 0°C ambient compared to 25°C. In addition, no detrimental environmental or biological effects for the manufacture or end use of the Westinghouse nickel iron battery system have been identified as a result of Environmental Impact and Safety Studies. A materials analysis indicates no significant raw materials impact will occur for annual commercial production of 25 kWh batteries in quantities of 100,000 units. Recycling of nickel is possible, with the most probable form being ferro-nickel alloys.

Progress during FY '80 has been substantial in the aforementioned areas of performance improvements and identified cost reductions. A solid base has been established to demonstrate cycle life and performance in electric vehicle systems during the next year.

2.0 TECHNICAL STATUS

The technical effort on the program during FY '80 was aimed at meeting the performance objectives of the program. These objectives and present performance levels are summarized in Fig. 2.1.

The objective of the System Development task of the nickel-iron battery program was to demonstrate improved performance capability in prototype cells, modules and battery. These improvements include: attaining 53-60 Wh/kg and 120-135 Wh/l in the overall cell, under 4-8h charge and 2-4h discharge conditions, while exhibiting short-term, stable cycling capability.

The System Development task encompasses five major subtasks:

(1) nickel electrode
(2) iron electrode
(3) cell components
(4) cell testing
(5) pilot plant operations.

The progress toward meeting the objectives of each of these subtask areas and their present status are now described.

2.1 NICKEL ELECTRODE

The nickel electrode development consists of:

- controlling electrode swelling
- improving active material utilization
- improving the load factor and porosity.

Concurrently, all these developments are aimed at reduced materials, processing and capital equipment costs.

Characteristics	Preliminary Contract Goals (Set Dec. 1977)	Best Present Demonstration
1. Battery Capacity (kwh) (100% rated)	25	26.5
2. Battery Dimension m H	0.28	0.28
(m H x m W x m L) m W	0.38	0.38
m L	2.21	2.21
Volume (ℓ)	230	230
3. Weight (kg)	417	420
4. Volumetric Energy (Wh/ℓ)	100	143
5. Specific Energy (Wh/kg)	60	58
6. Specific Power (W/kg)		
Peak Battery	100	175
Sustained @ C/3	20	--
7. Duty Cycle		
Charge (h)	4-8	C/3 for 4h
Discharge (h)	2-4	3
8. Lifetime		
Deep Discharges	2000	>500
9. Price/Energy ($/Kwh)	<60	--
10. Energy Efficiency (%)	>60	54

Figure 2.1. Nickel-Iron Battery Technical Goals

2.1.1 NICKEL PLAQUE

The nickel plaque refers to the current collector structure that is used both to contain the nickel electrode active material and to provide electrical conductivity to and from the electrode active material to the cell positive terminal. Presently, a double plaque is processed (Fig. 2.2), and is cut in half to produce the final nickel electrode. The plaque consists of steel wool that is nickel plated to provide corrosion protection to the steel fibers during the EPP process. The nickel plaque contains 2 vertical grooves that serve as electrolyte flow channels when the nickel electrode is installed into the cell stack.

2.1.2 EPP NICKEL ELECTRODE

The objective of this subtask is to improve upon the well-established Westinghouse EPP process for preparing nickel electrodes. Specifically, this effort is aimed at developing 25 Ah nickel electrodes with 0.25 Ah/g active material, 0.14 Ah/g total electrode and 0.075 Ah/cm^3, all at the 3h discharge rate. These goals are to be attained in plates of 2.54 mm maximum thickness. The EPP process technology, at the onset of this program, made 343 cm^2, 3.3 mm thick electrodes of the following specifications: 0.20 Ah/g active material, 0.12 Ah/g total electrode and 0.07 Ah/cm^2 at the 3h discharge rate.

In addition, electrode design and process techniques are being investigated to improve electrode dimensional stability during operation in a nickel-iron cell.

Experiments conducted to date show EPP, as applied to fiber plaque substrates, is most consistently accomplished by employing two levels of impregnation. These levels are: a) "high" current, followed by b) "low" current.

According to the concept arising from experiments, the "high" current step reaches a saturation level with respect to accomplished

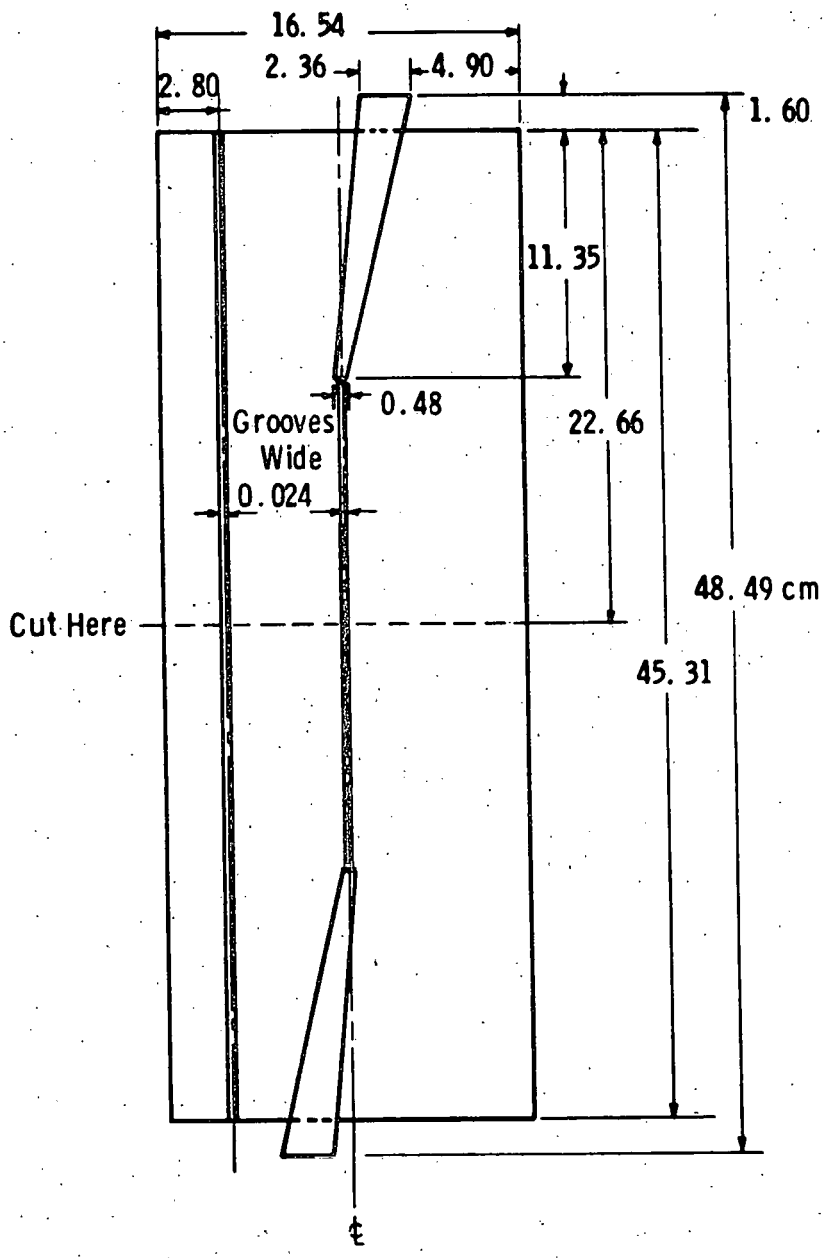

Figure 2.2. Nickel Electrode Plaque Design

impregnation with $Ni(OH)_2$ in a short time. The "low" current step, which is required to complete the $Ni(OH)_2$ loading to the densities needed for target capacity, can take from 16 to 20 hours to reach completion, as presently executed.

An increase in electrode capacity was accomplished by modifying the procedure between the two levels of EPP processing. The resultant electrode capacity is 25 Ah at a 2.5 mm electrode thickness. Total elapsed processing time is approximately 48 hours. This process has been employed for all nickel electrodes manufactured in the pilot plant during 1980.

2.1.2.1 COBALT SUBSTITUTION

Because of the potential shortage and sharply increased cost of cobalt on the open market, the composition of the nickel electrode was critically examined.. An important criterion for selection of candidate substitute materials is the crystal habit of the hydroxide species. It is reasonable to expect that candidate hydroxides should be crystal analogs of $Co(OH)_2$ if they are expected to replace $Co(OH)_2$ in its function as a capacity enhancer and cycle life extender for the positive electrode.

Known crystal analogs of $Co(OH)_2$ are: $Mg(OH)_2$, $Fe(OH)_2$, $Mn(OH)_2$, $Cd(OH)_2$. The order listed is that of relative unit cell volume, although other criteria, such as free energy of formation, metal ion radius or solubility in KOH may be more important properties. Since prior work at Westinghouse had indicated that barium was another possible replacement for cobalt, barium was also included in the investigation.

An objective was established to determine whether incorporation of these alternate materials in EPP processing, as distinguished from direct pasting methods which are also being considered, can equal or improve performance of nickel electrodes.

Calcium

Calcium in $Ni(OH)_2$ loaded electrode failed to produce the levels of performance that was expected. Work on calcium was not pursued beyond the 3-plate cell evaluation stages.

Barium

Barium did show promise as a possible cobalt substitute, and two 21-plate cells were put on test. Barium-to-nickel content in these electrodes was less than 1%, due to the low solubility of barium nitrate in the EPP solution (the loaded active material in the electrode tracks the Co:Ni ratio of the EPP solution). One cell was removed from test at 175 cycles, at which time the capacity had decreased to 160 Ah from an initial 195 Ah.

Iron

Iron also showed promise as a cobalt substitute in nickel electrodes made in the EPP process. In the case of iron, the solubility of ferric nitrate is sufficient to permit the formulation of an EPP nitrate solution. However, EPP nickel plaques processed in such a bath yield an active material containing a low iron:nickel ratio. This reflects, in this case, considerable preferential precipitation of nickel hydroxide over iron hydroxide from the bath.

Nevertheless, nickel electrodes containing iron, were prepared with a capacity of 22 Ah and a thickness of 2.44 mm. Three plate cells were cycled and dropped in capacity, dramatically, after 10-20 cycles. In order to compare with performance in a constrained cell, a 21-plate stackup was evaluated. This cell also lost capacity rapidly after 15 cycles.

Magnesium

Magnesium was the next cobalt substitute to be evaluated. EPP conditions for a co-precipitation of $Mg(OH)_2$ with $Ni(OH)_2$ were investigated.

An EPP bath, having magnesium nitrate and nickel nitrate was employed to produce magnesium-doped nickel positives.

Cell 091CE was constructed, cycled nine times and demonstrated a nominal capacity of 200 Ah at the 3-hour drain rate. In a manner similar to the tests on iron, capacity of this cell dropped rapidly after 10-15 cycles. It was removed from test at approximately 100 cycles, at which time its capacity was 120 Ah.

Summary - Cobalt Substitution

Co-precipitation of adequate amounts of the cobalt substitutes that were tried is difficult under any of the EPP process conditions. New methods need to be developed to achieve the requisite co-precipitation rates.

If these materials can be employed at all as cobalt substitutes, this should be ascertained by evaluating electrodes having a nominal ratio of Nickel:Mx, where Mx denotes the candidate cobalt substitute material. This can be done most easily by preparing electrodes via the pasting route, rather than by EPP, at this time.

2.1.2.2 NICKEL ELECTRODE EXPANSION

An important design problem related to cycle life of the nickel-iron cell is the stack electrolyte starvation resulting from an increase in the nickel electrode thickness on cycling. The design approach under development and evaluation to circumvent and/or minimize EPP electrode swelling is, basically, a high-strength, low-loading, high active material utilization electrode, via a high fiber density plaque design.

Nine EPP runs, comprising 108 electrodes, were processed to evaluate the effect of grid fiber density on electrode performance. The data for electrodes having a nominal 2.54 mm thickness were extended further, to plots of specific nickel active material efficiency versus the ratio of active material (AM) volume ÷ current collector fiber volume.

Relative grid fiber has been incrementally raised. A trend to greater AM efficiency may be present due to increased pore volume but the data are not precise enough to resolve this effect very clearly. The results have demonstrated that more active material efficiency results when higher fiber density (low AM ÷ Grid) plaques are employed.

To demonstrate these results, cell 048CE, employing higher fiber density, was constructed and cycled to establish the relative merit of high fiber density on performance, particularly, electrode swelling.

Discussion: Cell 048CE (High Fiber Density) Results

Cell 048CE, which reached end-of-life after 258 charge-discharge cycles, exhibited much less nickel electrode expansion than is normally observed. The electrodes from this cell were originally 2.44 mm thickness. When removed from the case, they averaged 2.67 mm. Expansion up to 3.05 mm had been observed for electrodes having several hundred test cycles. The critical design aspect of this cell was a higher fiber density. Needle-punching was not employed for these particular electrodes.

Failure of this cell is attributed to stackup dryout. After 258 cycles, wet-weight determinations indicated that active material volume percent had increased, before release of compression. This resulted in a decrease in porosity, a change that was insufficient of itself to account for the unsatisfactory stackup wetting with electrolyte.

The increase in active material weight and volume on Cell 048CE may result from two processes:

(1) $Ni(OH)_2$ lattice incorporation of K^+ and Li^+ ions and, possibly, incorporation of additional water of hydration in the crystal lattice.

(2) Addition of $Ni(OH)_2$ and $Fe(OH)_2$, due to corrosion of both the nickel electrode and of the exposed steel fibers of the grid.

Since significant corrosion of the nickel plating on the steel fibers has been observed by microscopy on extensively-cycled fiber plaques, mechanism (2) is quite important. Of the total of 30g typical weight pickups per electrode measured after cycling, analysis shows that only 10g can be attributed to alkali metal ion absorption. The remainder must be due to either chemically-bound OH^- ion, attached to the corroded fiber grid material, making mechanism (2) dominant on pickup of water of hydration.

Chemical analysis shows that, after 258 cycles on Cell 048CE, the active material contains approximately 3.0 w/o iron, further corroborating the view that fiber corrosion has taken place. In spite of this growth of additional $Ni(OH)_2$ and $Fe(OH)_2$ material within the nickel electrode, a steady decrease, not an increase, in capacity was observed. Decreasing porosity serves to hinder electrode performance, although the 5 v/o porosity decline estimated in this case would not seem to be the strongest influence.

Instead, at least two other mechanisms should be considered:

(1) progressive loss of electrical contact due to the formation of a corrosion scale,

(2) "poisoning" of the active material with iron.

Since the original Edison cell delivered long cycle life with nickel flake as the current collector, then mechanism (2) would appear to be most plausible. Details of the "poisoning" mechanism are unclear, but the effect of iron has been suggested to be one of lowering charge voltage. Therefore, further work was then oriented toward improvement of the coverage and bonding of the protective nickel plate over the steel fiber current collector. The throwing power of the plating bath can be improved by adjusting current density to lower values and employing, correspondingly, longer plating time. This approach was evaluated in a development nickel plating process line.

2.1.2.3 NICKEL-PLATING EXPERIMENT

Cell #80 (21-plate) had been constructed with high-density fiber plaques having needle-punched construction and an extended nickel-plating time. The nickel plating current was reduced, keeping plated nickel weight constant. Thus, this specimen should have demonstrated advantages that could be derived from a more uniform nickel plating on the steel fibers. Initial capacity for the electrodes on the EPP rack was 23.9 Ah/plate. Initial capacity of the cell was 230 Ah. At 150 cycles, the cell delivered 180 Ah at the 3 h rate.

Further experiments were carried out with longer nickel-plating times and lower plating current densities. The resultant plaques were, mechanically, quite weak, indicating that a very low-current density, cathodic protection was insufficient, with respect to bath condition to prevent steel fiber corrosion in the acidic plating solution.

2.1.2.4 HIGH FIBER DENSITY GRID STRUCTURE

The evaluation of grid structures with heavier fiber weight is being continued. Seventy electrodes with the heavier grid were fabricated in the EPP pilot line and processed through cell assembly and

testing. Seven 21-plate cells were tested to evaluate the merit of heavier fiber plaques. The results are summarized below:

Plate Thickness (mm):

Min	Max	Avg	S.D.
2.37	2.49	2.41	.04

Active material weight ---------- 89 g/electrode
Capacity for a 70-Plate Rack ---- 23 Ah/electrode (average)

Initial (3-hour drain rate) capacities of these cells were determined on the formation bench:

	CELL NUMBER						
	084CE	085CE	086CE	087CE	088CE	089CE	090CE
Cycle #1 (Ah):	190	223	204	208	212	206	214
Cycle #7 (Ah):	210	227	208	212	221	213	227

A six-cell module, employing these cells has been constructed and was cycled on the module tester to compare performance versus standard-design cells. One cell developed a short, creating a high-temperature spot on the bottom of the cell and affecting the two adjacent cells. The test is being continued with the remaining three unaffected cells.

2.1.2.5 GAS PRESSURE RELIEF EXPERIMENTAL DESIGN

Based upon the ongoing work on nickel electrode designs, a concept has been developed to permit gas pressure relief during the charge cycle. Additional electrode height has been incorporated for selected electrodes in the nickel-iron cell stackup design. These higher electrodes will extend into space that is presently not utilized above the stackup. Because of greater separation distance, this portion of the

positive and negative electrodes will not employ separators. The exposed electrode surfaces are expected to gas freely on overcharge, thereby preventing stackup dryout and plate swelling. Also, the design should provide approximately 4 Ah additional capacity in the planned 21-plate test cell. These special electrodes have been fabricated and cell construction completed (Cell 093CE). To date, at 32 cycles, this cell is stable at 215 Ah at the C/3 drain rate.

2.1.2.6 "BRUSH" ELECTRODE SUBSTRATE

The electrode substrate comprises radially-emanating current collector fibers, oriented about a steel wire bus axis. Many of these components, comprising individual "brushes" are arranged in parallel, vertically, and connected to the top bar and tab (Figure 2.3).

This type of brush design (axially-oriented fiber) is uniquely suited to the EPP method of impregnation. Such a design, by virtue of the fiber orientation, should display both maximum resistance to electrode expansion in the thickness direction and enhanced power capability.

Since the starting brush fiber material is cotton, the nickel plating of this structure has, in the past, involved an electroless nickel "flash" coat, followed by conventional electroplating. An alternate method has now been devised in which the cotton fibers are rendered conductive with a heat treatment. This carbonaceous conductive structure is easily electroplated directly, thereby eliminating the electroless nickel plating operation. The structure employed in this design has aspects which comprise improvements in critical areas:

(1) Electrical contact to the active material is via nickel whiskers with a carbon core, thereby reducing possible iron contamination of the active material and/or fiber breakage when steel fiber corrosion can occur.

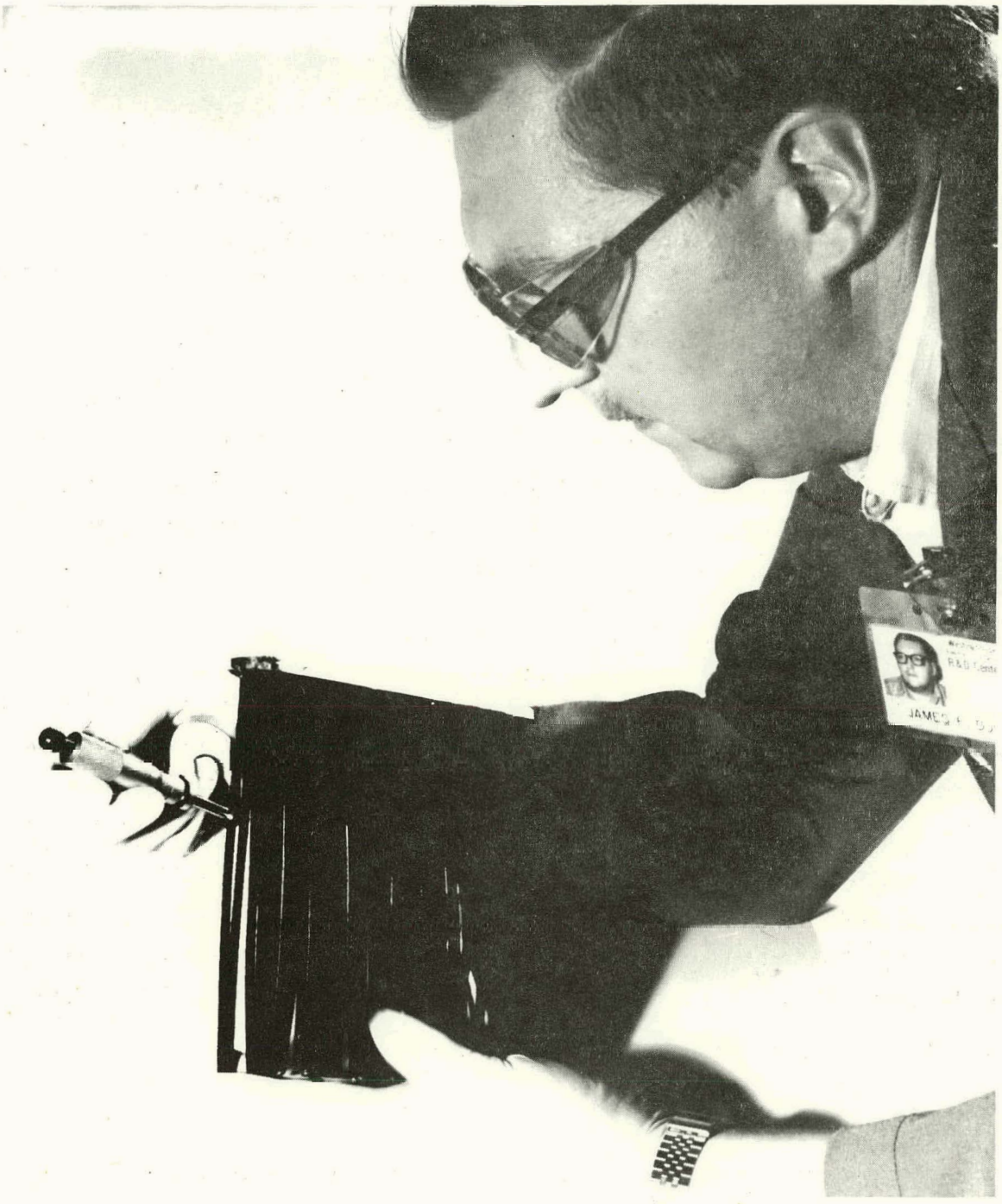

Figure 2.3. Full Size "Brush" Type Nickel Electrode

(2) Radial fiber/tubular design, with much less possibility of expansion, compared to random fiber orientation in state-of-the-art plaques.

(3) Reduced average mean free path from active material to the current collector providing, potentially, more power capability than the standard EPP electrode.

Therefore, the next generation brush-type design, comprising nickel plating directly over carbon for the entire electrode could provide improved positive electrode cyclic stability. Due to the emphasis of work in the area of sintered steel wool plaque strengthening, the brush type electrode activity is presently suspended.

2.1.3 PASTED NICKEL ELECTRODE

The performance goals for the pasted nickel electrode are the same as those cited for the EPP nickel electrode. However, independent preparation of active material and subsequent pasting into the plaque can offer a reduction in total electrode manufacturing cost and significant decrease in capital equipment expenditure, relative to the total EPP process. Effort during the past year has centered on methods for continuous, large batch production and formulation of an optimum active material paste composition, for incorporation into the nickel plated fiber metal plaque.

2.1.3.1 PREPARATIVE METHODS

Two development approaches are currently being used for the production of nickel (paste) active material. The first approach involves the incorporation of commercially-available green nickel hydroxides into the nickel plated steel wool plaque. These commercial materials have a density of 3.5 to 3.7 g/cm^3 and electrode active material loadings of 90-100 g in 345 cm^2 area are achievable at 2.0 mm final thickness.

Additives, such as cobalt hydroxide, are milled with the nickel hydroxide prior to the paste making operation.

A second development approach for the production of nickel active material involves the room temperature ozonation of alkaline slurries of nickel hydroxide or carbonate. The ozone stream converts the nickel species into a black, flocculant powder of lower density than the initial green powders. This lower density results from incorporation of alkali cations and water molecules into the nickel-oxygen interlayer during the ozonation process. These black powders require only a few charge-discharge cycles to achieve maximum electrochemical utilization. The composition and structure of the active material prepared by using this method is very similar to that obtained as a final product in the thermal process. In the ozonation process, the pH of the slurry can either be neutral, or slightly alkaline, without affecting the performance significantly. Strongly alkaline slurries (>pH 10) tend to decompose the ozone and thus require longer ozonation time.

The ozone reaction chamber that is currently in use is pictured in Figure 2.4. The unit was constructed in house and is modeled after the York-Schriver liquid-liquid extraction column. It consists of a vertical chamber separated into eight reaction zones, each consisting of a pair of baffle plates and a stirring paddle. Each baffle plate has a center hole and the lower baffle of each pair is extended to the glass chamber wall by a teflon skirt. Ozone enters the cylinder through a perforated ring at the bottom so that bubbling lifts the slurry. The counter effect of gravity results in a circular agitation in each zone. A drain at the bottom allows easy removal of active material. New material is then entered through a top fill hole connected to a pump and reservoir. Continuous pilot production of active material can be achieved, by using this apparatus, for evaluation in full-size cells.

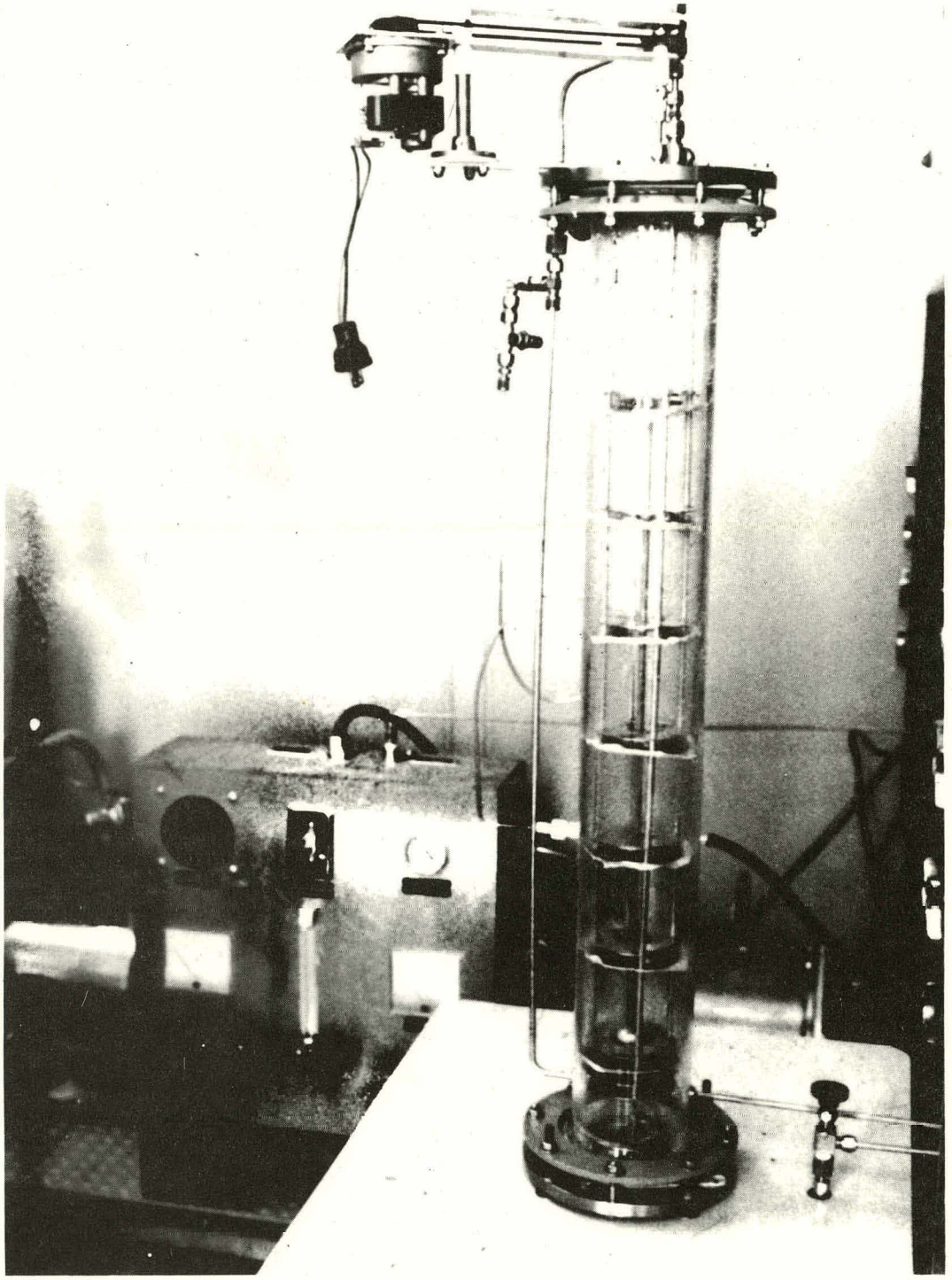

Figure 2.4. Eight Zone Ozonation Chamber

2.1.3.2 ELECTRODE CONSTRUCTION

Nickel active material is loaded into a fiber metal plaque, using a roll pasting procedure similar to that used for the iron electrode. To assure uniform distribution and reproducibility of loading, the aqueous paste must maintain single phase fluid properties during rolling. Suitable deflocculants, which do not affect active material performance, are added to the paste to prevent curdling. At this step, cobalt hydroxide, or other performance improving agents, are incorporated.

The performance goals for pasted nickel electrode in the nickel-iron battery is 0.14 Ah/g of finished electrode at the C/3 discharge rate and at a 25% overcharge. A large number of full size electrodes (344 cm^2) have been constructed and tested in order to meet the goals required for a finished cell. The pasting procedure begins with plaques about 4.5 mm thick which are then roll pasted, dried and sized to 2.5 mm, or less. Loadings of 90-105 g active material per full size plaque are achieved at 1.8 to 2.3 mm final sized thickness. These have a resulting electrode performance in the 20 to 23 Ah range over hundreds of test cycles.

2.1.3.3 ADDITIVES

Cobalt hydroxide continues to be the best additive to enhance the performance of pasted nickel electrodes. Addition of $Co(OH)_2$ to the active powder enhances utilization 20 to 30% over nickel hydroxide alone. Due to the cost of cobalt, other additives are under investigation. Known crystal analogs of $Co(OH)_2$ were tried initially. These, included $Mg(OH)_2$, $Mn(OH)_2$, $Ca(OH)_2$, $Ba(OH)_2$ and their peroxide forms. These additives were milled with the nickel powders, prior to the paste making procedure. No significant effects in performance were noted for these additives at various concentration levels. Other materials under investigation include: aluminum, chromium and their mixed metal oxide analogs.

2.1.3.4 FULL-SIZE CELL CONSTRUCTION

Full-size cells, constructed using pasted nickel-electrodes, have achieved hundreds of stable,high performance cycles. Emphasis now is on production of additional cells, using both green nickel hydroxide and ozonated active material. These cells will encompass many process variables, including electrode thickness and additives other than cobalt hydroxide.

Nickel electrode thickness increase on prolonged cycling is the most important factor in determining life and performance of the nickel iron cell. Pasted nickel electrodes offer greater flexibility and control over electrode parameters. Uniform loading, optimum porosity and fixed final thickness can be effectively achieved and their influence on long life can be determined. Cells are bing constructed with nickel electrode thicknesses varying from 1.80 to 2.30 mm. Cell life will be determined as a function of these initial thicknesses. Both active material types are being used in these experiments.

2.2 IRON ELECTRODE

The composite-type iron electrode contains a fiber metal-expanded metal combination conducting grid system as the current carrier. This structure allows firm attachment of the connecting tab and imparts excellent power characteristics to the iron electrode. The battery design requires an iron electrode of 345 cm^2 active area and approximately one mm thickness, having an output of 26.5 Ah at the C/3 discharge rate. The final program goal is to achieve 0.27-0.28 Ah/g of total electrode, entirely on the upper voltage discharge plateau.

2.2.1 IRON PLAQUE

The current collector for the iron electrode is a porous structure, presently formed from a combination of steel fibers and an expanded metal iron sheet. The expanded metal is the center layer for the fiber

structure which is sintered to both sides using a similar fiber lay-up as developed for the plaque used for the nickel electrode. The final plaque is sintered in hydrogen and a vertical tapered tab is seam welded into the plaque body (See Fig. 2.5). The open pattern in the expanded metal is diamond-shaped and the long direction, having higher electrical conductivity, is aligned with the axis of the fiber. A process advantage of this composite grid structure is that the expanded metal center provides integrity in handling the plaque during the seam welding operation.

The basic process steps in the continuous production of full size electrodes are: (1) the loading of the grid structure with red iron oxide and carbon additive. (2) the reduction of this mixture and (3) the pressing of the electrode to a final thickness of 1 mm. Control over the amount and uniformity of the loading is based on the expansive structure of the steel wool matrix and on the use of a suitable paste of the oxide.

After the pasting step, a room temperature drying step is required to remove most, or all, of the paste water. An open structure results, which offers easy access for the hydrogen gas during the in-situ reducing step. A continuous belt hydrogen furnace is used for the reducing procedure. The overall dimensions of the electrode are not affected by the reduction step. The final electrode contains a 68-70 g loading and is readily pressed to 1.0 mm.

2.2.2 COMPOSITE ELECTRODE

The starting material for the composite-type iron electrode consists of red iron oxide and a carbon-producing additive, such as phenolic resin, or most recently, corn starch. These components are incorporated as an aqueous paste into the steel wool grid, as described previously.

Overall electrode performance is strongly dependent on the properties of the red iron oxide starting material. Initially, successful results were obtained using Fisher Red Iron Oxide which is prepared by calcining ferric sulfate. Some residual sulfate (0.05 wt%) remains after

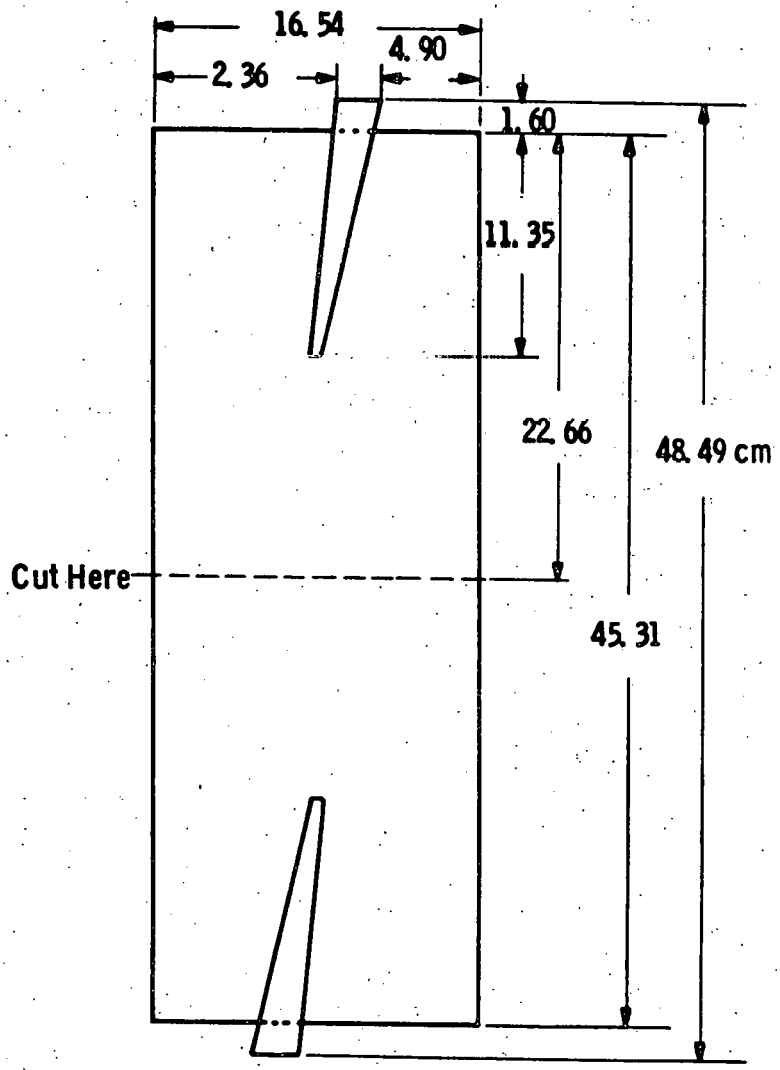

Figure 2.5. Iron Electrode Plaque Design

calcination and this imparts a degree of catalytic activity to the iron oxide. Prior research and development efforts indicate that the ferric sulfate calcination temperature is the most important factor in determining final electrode performance. A summary of electrode performance versus calcination temperature and residual sulfate concentration was included in the 1979 annual report.

Several suppliers were contacted to provide iron oxides to the required specifications. Experiments with certain Pfizer and Columbian Carbon calcined red oxides yielded 25-30 Ah in full size electrode tests. These electrodes exceed the 23-25 Ah performance achieved using the Fisher oxide and cost approximately 1/3 that of the Fisher Red Oxide. In the past year, material was obtained in ton-lots for use in battery manufacture. Electrodes prepared from this Pfizer material consistently exceed 26 Ah per full size electrode at the C/3 discharge rate. The Pfizer electrodes have shown no significant loss in capacity after 500 cycles of continuous testing.

Evaluation of several types of carbon-producing additives has been completed in full-size electrode tests. The materials found most effective, initially, were phenolic resins of the phenol-formaldehyde type. These materials lose weight when reduced in hydrogen and leave behind a carbon residue evenly distributed throughout the electrode active mass. This carbon residue was found to increase electrode performance about 20%, compared to iron oxide with no additive. Some eventual storage problems, particularly caking, occurred using this material. Further experiments led to the selection of corn starch as an additive which had all the desired properties for paste formulation and handling. Addition of corn starch to the iron oxide paste produces electrodes which meet the performance and life obtained using the phenolic resin.

New pressing techniques have recently been incorporated into the iron electrode sizing process, resulting in significant capacity increase. All processing parameters and raw materials are the same, as

specified in the preceding paragraphs, except for the final sizing step. These new process iron electrodes are sized, using 0.97 mm shimstock and a fabric interface between the electrode and the face plates of the press. This interface prevents closing of metallic iron pores at the electrode surface during pressing, thereby allowing better electrolyte access to the electrode interior when placed in a cell stackup. Performance is 28-29 Ah, versus 24 Ah for electrodes pressed in the former manner without shims and fabric. The 28-29 Ah capacity results from a constant current charge input of 33 Ah (4 hr x 8.3A) for an Ah efficiency of about 87%. This high coulombic efficiency should enable high energy efficiency to be obtained (~70%) in nickel-iron cells built with these electrodes.

The curves in Fig 2.6 represent Ah capacities at about 0.80 V (vs Hg/HgO) terminal voltage for the iron electrodes. If only 25 Ah is removed from these newer technology electrodes, the final voltage is about 0.86 V (vs Hg/HgO). Since the starting voltage is about 0.92 V (vs Hg/HgO), the total drop for these iron electrodes in a 250 Ah cell is Δ 60 mV. This value exceeds the original program goal of Δ 80 mV and should aid greatly in improving the thermal characteristics, internal resistance and charging efficiency of cells, since these iron electrodes are now operating on the higher portion of the voltage discharge curves. Specification for these improved iron electrodes are given in Table 2.1.

Further improvements in iron electrode performance can be expected with optimization of the oxide starting material and refined pressing techniques. These areas are being explored to achieve a goal of 32 Ah output.

2.2.3 LIFE TESTS RESULTS

Full size iron electrodes were put on continuous test in January 1979 to determine the effects of all components on electrode life. The variables included nickel plating of the steel wool matrix, carbon

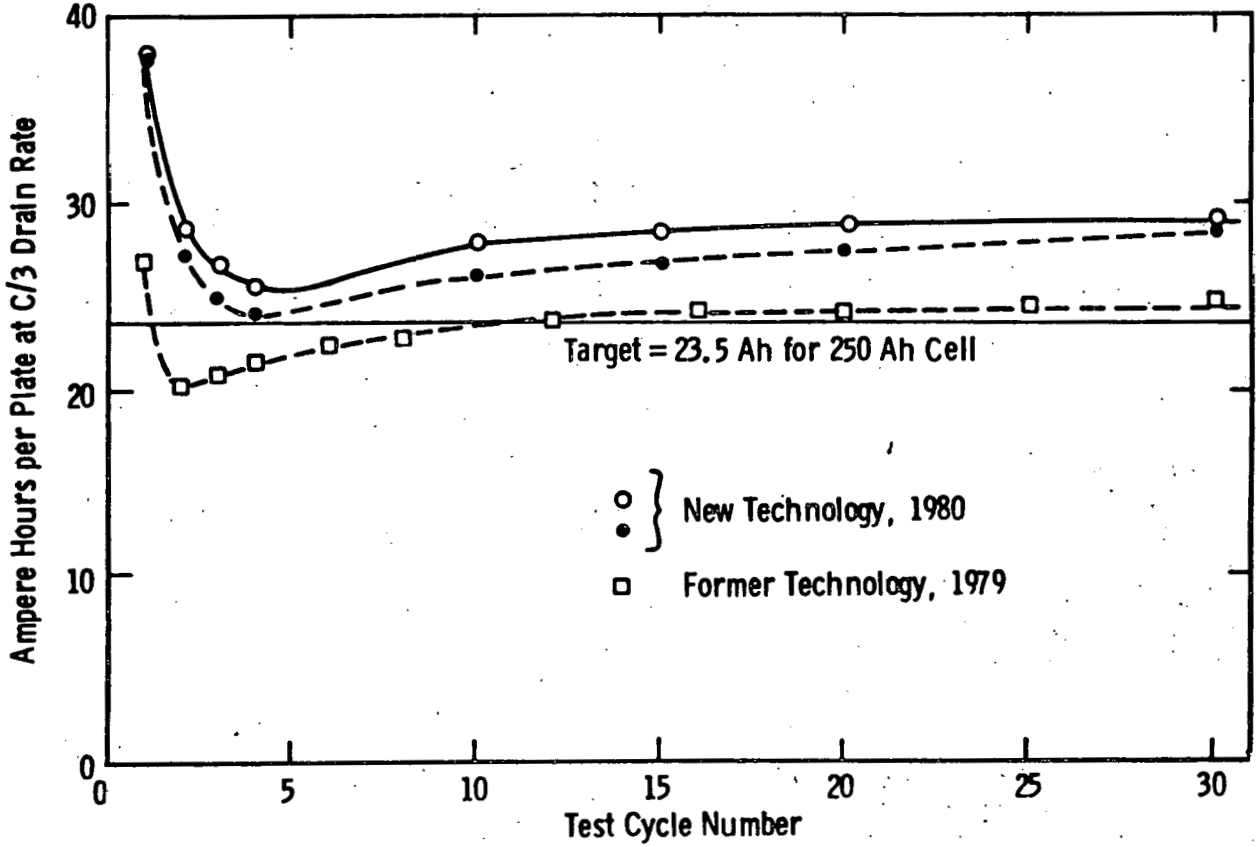

Figure 2.6. Iron Electrode Performance

TABLE 2.1

IRON ELECTRODE SPECIFICATIONS

Thickness	Program Goals 1.0 mm (40 mils)	1979 1.0 mm	Present - 1980 1.0 mm
Weights for 11 electrodes (g):			
Grid & Tab	493	493	493
Active Material	750	770	770
Active area (cm^2)	343	343	343
Performance at C/3:			
Ah	25	25	29
Ah/g active	0.34	0.34	0.40
Ah/g electrode	0.22	0.22	0.25

additive content of the active material, tab configuration, and size of the steel wool fiber. All experiments were run using Fisher Red Oxide, since that was the raw material at that time. These tests were designed to give insight into the reliability of these components over 1000 test cycles. A summary of test results is given in Table 2.2.

Electrode FX901 was removed from test at 725 cycles after its performance had declined to 17.3 Ah. Examination revealed that the unplated steel wool matrix was severely corroded and had separated from the expanded metal center grid. The vertical tab remained firmly attached to the expanded metal grid. The active material was very soft thoughout the entire electrode. The electrode had expanded to 1.40 mm from the initial 1.00 mm value. Failure was related to steel wool corrosion and the resulting detachment of active material from the electrode body.

Electrode FX902 was removed from test at 418 cycles since the capacity had fallen below 18 Ah at the C/3 discharge rate. Failure was attributed to the iron electrode. Electrode FX902 contained unplated steel wool fibers and had a horizontal tab connection. A steady decline in performance was noted after 350 cycles and the electrode was removed at 418 cycles where it had an output of 15.7 Ah. The active material for this electrode contained no phenolic resin. Examination revealed that the body of the electrode maintained its metallic appearance and original thickness with no noticeable corrosion of the steel wool fibers. Some deterioration at the tab junction was apparent and would account for the observed decline in the discharge voltage.

Electrode FX903 was removed at cycle 412 with an output of 17.2 Ah. The active material throughout the entire electrode was mushy, although the fibers appeared intact. The electrode had swelled to about 1.9 mm from its original 1.0 mm thickness. This is in contrast to FX902, which maintained its active material integrity over a similar number of cycles. The basic difference between these two electrodes is that FX903

TABLE 2.2

CYCLIC STABILITY OF COMPOSITE IRON ELECTRODES

	Active Material Wt. g	Electrode Wt. g	Ah Capacity vs. Cycles 5	10	50	125	500	1000
FX901	69	120	21.9	24.2	24.3	22.9	21.9	17.3 (off at 725)
FX902	67	115	17.5	19.1	23.6	20.6	15.7 (off at 418)	
FX903	69	116	24.6	24.7	24.5	20.0	17.2 (off at 412)	
FX904	70	120	24.9	25.1	24.7	22.6	21.8	18.0 (off at 960)
FX905	71	124	17.6	21.1	22.4	17.2	21.7	18.0 (off at 1050)
FX906	66	113	13.7	22.6	24.3	22.1	22.1	18.0 (off at 1150)
FX907	69	115	19.3	22.9	23.0	20.9	18.0 (off at 160)	

Active area = 53.2 in^2 = 345 cn^2

Thickness = 40 mils = 1 mm

Electrodes are Fisher Red Oxide

Electrodes are discharged versus nickel counter electrodes to a final cell potential of 0.97V for each test cycle.

contained phenolic, compared to none for FX902. However, FX901, 904 and 906 also contained phenolic and continued to perform well at 500 cycles.

Electrode FX904 declined to a steady output of 18.0 Ah and was taken off test at 960 cycles. This electrode contained a nickel plating on the fibers and tab and also contained phenolic in the active material. Evaluation of this electrode revealed that the active material remained intact and that no significant thickness increase had occurred. The average discharge voltage had decreased about 50 mV from its optimum value in the first 500 cycles. Some very thin cracks were observed along the length of the electrode body. Constant expansion and contraction of the nickel counter electrodes most likely caused the cracks to occur, resulting in fatigue and voltage loss. Electrode FX905, removed from test at 1050 cycles, was similar to FX904.

Electrode FX905 was removed from test after 190 cycles since its capacity had declined to 17.2 Ah. Cell voltage profiles indicated that the nickel electrodes were limiting performance. The nickel counter electrodes were of prior design. New nickel electrodes were inserted and testing was resumed. An immediate increase from 17.2 to 21.7 Ah was obtained. Simultaneously, new counter electrodes were inserted in all the test cells. Unfortunately, it was too late to rebuild electrode FX907 which was removed a few weeks earlier.

Electrode FX906 declined to a steady 18.0 Ah output at 1150 cycles. The failure mode for this electrode was ascribed to some fiber weakening and resulting loss of active material integrity. The electrode body was still adequately attached to the horizontal tab.

Electrode FX907 was removed from test at 160 cycles at a capacity of 18 Ah. This electrode contained unplated steel wool fibers and phenolic resin. No measurable expansion from the 1.00 mm (initial) thickness was observed. This electrode retained its hard and smooth tab junction. A steady decline in average discharge voltage accompanied the decrease in output. No corrosion in the main body of the electrode was observed. It

possible that degradation at the tab junction contributed to the 20% decline in capacity observed for this electrode.

It is concluded from these tests that the sintered composite type electrode is capable of long life (>1000 cycles) in nickel-iron cells. Since these tests were begun in January 1979, several improvements have been made in tab welding and grid structure integrity. These, along with changes in active material composition, have increased performance dramatically, as described previously. Electrodes manufactured using this newer technology are currently on life test and are approaching 600 cycles with capacities greater than 25.0 Ah, representing less than 5% decline from their optimum values. Nickel plating of the grid structure is now considered not necessary for long life iron electrodes since 1500 cycles are obtainable, using the newer technology approach.

2.3 CELL HARDWARE COMPONENT DEVELOPMENT

Development work on cell components includes: separator(s), cell and intercell connectors, cell case and cover, and cell auxiliaries that deal with automatic water feeding and/or the electrolyte circulating system.

2.3.1 SEPARATORS

A decision was made to use Celgard K-501, supplied by Celanese Fibers Company, as the standard separator. This decision was made because of the satisfactory performance of cells in which it was used and because of its good handling properties. In particular, since it is laminated into one sheet, adoption of a serpentine method of wrapping electrodes in the stack assembly was possible. One shipment was received with high resistance K-501, caused by excessive wetting agent, but this was replaced by Celanese with acceptable material. The quality control measurements made on incoming material are given in Table 2.3.

TABLE 2.3

QUALITY CONTROL MEASUREMENTS ON CELGARD K-501

Roll No.	Thickness Mils	Weight g/yd^2	Resistance[1] $m\ \Omega\text{-}in^2$
6723*	13.3	69.9	77
21846	14.3	69.9	29.5
21847	14.2	70.1	31.5
6721*	13.1	72.5	646
832-7-1*	10.9	70.5	889
839-1-2*	13.3	82.4	1136
839-4-1	13.1	74.8	1106
874-4-2*	14.0	88.3	674
855-8-1*	12.3	80.2	770
854-4-1*	12.8	70.1	816
6727*	13.1	75.6	677
23294	14.2	70.0	32.5
23295	13.8	70.7	34.6
23296	14.9	71.9	30.6
23297	13.0	74.1	29.3
23298	13.9	72.0	29.6
23299	13.1	71.4	29.8

(1) Separator resistance is measured by the ac method, described in Alkaline Storage Batteries, by Falk and Salkind, pp 257-260.

* Returned to supplier.

In the search for an alternate separator to K-501, barrier and absorber materials from W. R. Grace Company were evaluated. This was done by comparing measurements and performance of the W. R. Grace materials with those of Celgard K-501 and its components, Celgard 3401 and Fibertex. An advantage of W. R. Grace barrier is that it has, potentially, a much lower price than Celgard 3401. The thickness, weight and resistance measurements are shown in Table 2.4.

TABLE 2.4

COMPARISON OF W. R. GRACE AND CELANESE SEPARATOR MATERIALS

Supplier	Material	Thickness (mils)	Weight (g/yd^2)	Resistance ($m\ \Omega\text{-}in^2$)
W. R. Grace	90921-BC-1 barrier	7	136	20
W. R. Grace	114 absorber	6	63	10
Celanese	K-501 laminate	13.2	71	30
Celanese	3401 barrier	1	11.3	5-10
Crown Zellerbach	Fibertex absorber	5.8	26.4	7.1

Two 21-plate cells were assembled with the W. R. Grace materials, and two control cells were assembled with Celgard K-501. The serpentine method of assembly is too difficult to use with the unlaminated W. R. Grace materials, therefore the bag type of construction was used. These bags were made with one layer of absorber and one layer of barrier, the absorber being inside the barrier; the bags were assembled on the iron electrodes. Bags were also made of K-501 for the iron electrodes of the control cells, thus the type of assembly used for separators in all four of the test cells was the same.

On the initial charge-discharge test cycles the capacities of the cells were similar but, by cycles 7 and 8, the average capacity of the

control cells was 20 Ah greater than the capacity of the cells with W. R. Grace separators. Internal resistance and pressure readings on the cells with W. R. Grace separators tended to be higher than on the cells with Celgard K-501. The capacity of the experimental cells was limited by the iron electrodes, which may have been affected by reduced access of electrolyte to these electrodes.

Therefore, K-501 is the present "standard" separator for nickel-iron cells. However, exploration and examination of other candidate separator materials, as they become available from the commercial suppliers, will continue.

2.3.2 ELECTRICAL CONNECTORS

The continuing objective of this subtask is the development of reliable, easily manufactured and highly conductive electrical connectors. The connectors interface with two types of environment -- the internal connections (requiring caustic-resistant components) and the connections external to the cell (in air). The present internal design for the cell terminal assembly is a four component system, involving three joints: (1) electrode-to-tab, (2) tab-to-collector and (3) collector-to-terminal post, with experimentation being conducted on joining materials and/or techniques. The external intercell connections are lengths of flexible cables, with mechanical fastener joints at each end, that clamp onto the cell terminal posts.

The internal connections between the electrode tab and the terminal post have received much attention during the past year. Here development work was focussed in two major areas: (1) cost reductions in comb fabrication, and (2) elimination of the tab and comb. Significant results were seen in (1) where combs were assembly welded (rather than machined) from individual blanks and bar stock pieces. Preliminary work in (2) involved a technique that utilized cables and a through-the-cover cable collection terminal.

The cost savings achieved in the assembly welding of combs led to the method now being used. Here a bar stock piece is first spot welded to each electrode tab in an operation that eliminates the melt down of separator at the tab region on top of the plates, which was always a problem when the machined comb was welded to each electrode tab, despite various heat sinking schemes that were employed. Later, during cell stack assembly the electrodes are gathered and welded to the collector assembly (See Fig. 2.7). This not only reduced the cost of the assembly but improved the stacking operation. The second development activity was no longer necessary and was discontinued.

2.3.3 CELL CASE AND COVER

Work in this area was two-fold: (1) design and procurement of molded prototype cell containers and covers, (2) development of new joining and sealing techniques, having compatability to a multicell module case and cover.

A new design of case and cover is being utilized. Improvements in the circulation ports and the external connections associated with them necessitate changes in the cover, as shown in Fig. 2.8. At the same time, structural changes were made to strengthen and improve the seal integrity of the area around the terminals. The case design finally selected remains very close to the original. Previous core shift problems were resolved by tighter alignment during the mold setup.

The induction weld sealing process (cover-to-case) was also abandoned. Dimensional variations in the adjoining pieces, although satisfactory for an adhesive method, proved too large for the sensitive induction equipment. Burns and leaks in the joint area were unacceptable.

A conceptual design for a multicavity module was completed. The aim was to reduce the volume and weight of a six-cell module by packaging all as a group. Additionally, manifolding and intercell connections were

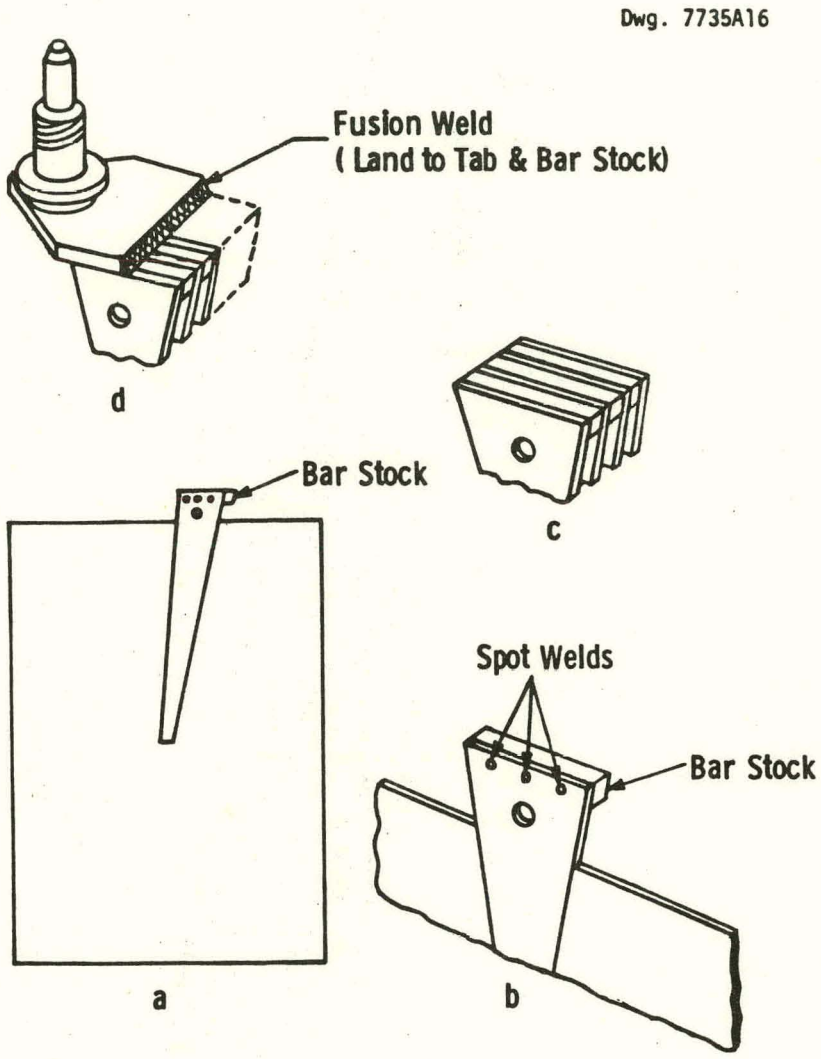

Figure 2.7. Electrode Tab Weld Assembly

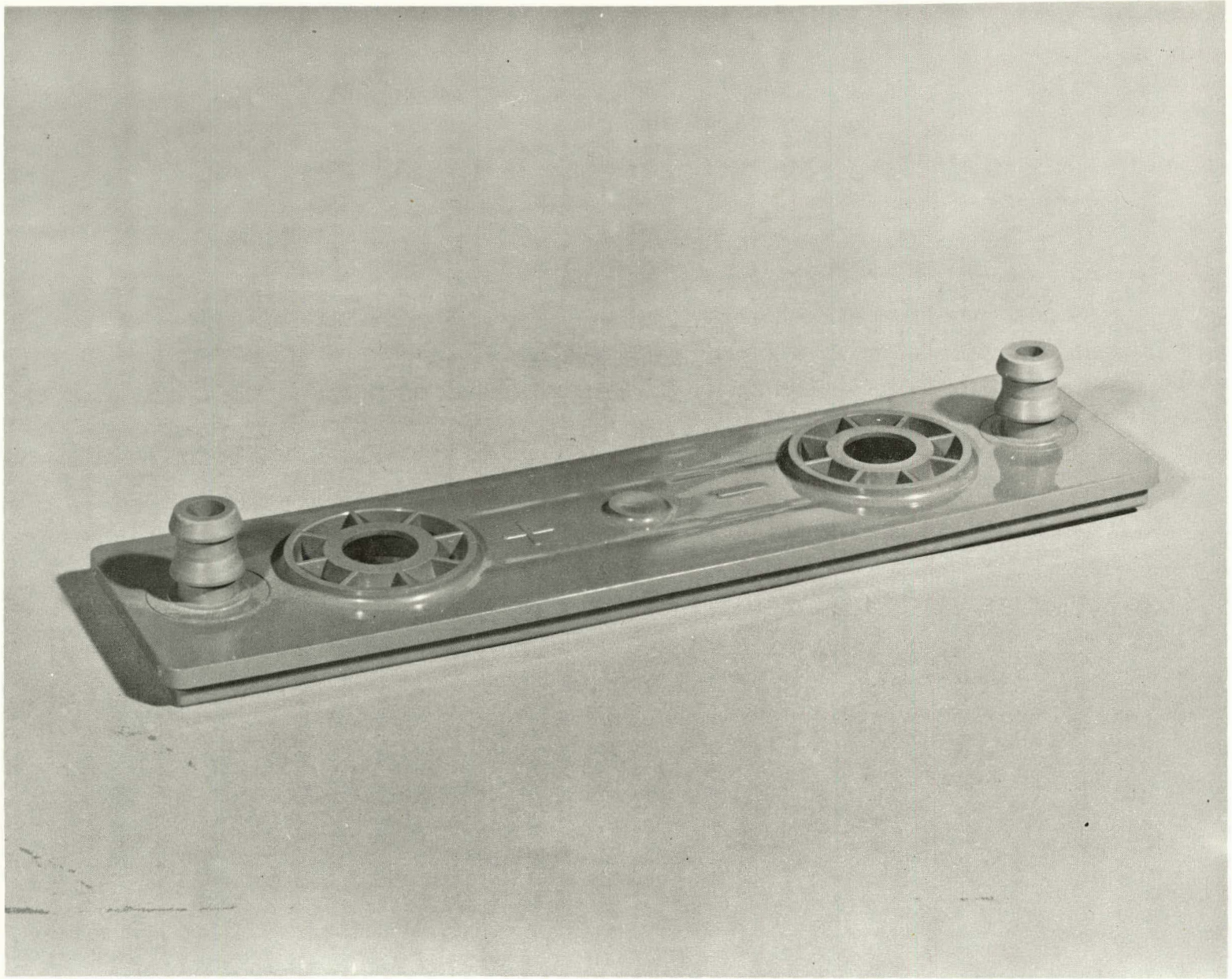

Figure 2.8 Cell Case Cover

made internally. Figure 2.9 shows the design. Here, about 9% reduction in weight and 14% in volume can be achieved.

2.3.4 ELECTROLYTE MANAGEMENT SYSTEMS

Development work on auxiliaries relate to electrolyte water makeup and electrolyte recirculation. Emphasis is on an automated system capability.

An electrolyte management system (EMS) has been developed to provide minimum maintenance features through single point water replenishment, charge temperature control, and safe gas handling. Electrolyte circulation through the battery during the charge cycle provides effective heat removal thus enabling 2-5 hour charging and cooling of a 100% discharged battery. The primary elements of the EMS are pump, reservoir, heat exchanger and associated flow controls and interlocks. Development work during the past year was concentrated on design of a system for on-board vehicle use. Several improvements have been made in the safety and reliability of the electrolyte management system, including flow, level, temperature and spill protection. The integrity of the fluid seals at the cells has also been increased. The manifolding has been changed to incorporate flexible feed and exhaust hoses and elastic seals, making the system not only less sensitive to motion and misalignment stresses, but also more suitable for cell interchanging. Leaks at the manifold/cell joint have been completely eliminated. Fig. 2.10 shows a flexible hose manifold attached to a cell string.

2.4 CELL TESTING

The purpose of the testing program is to demonstrate the state of technological advancement, with respect to the overall nickel-iron battery goals. The ultimate purpose of the testing program is two-fold: (1) provide performance information for use by the developer as feedback to determine operating characteristics, suggest modifications, and

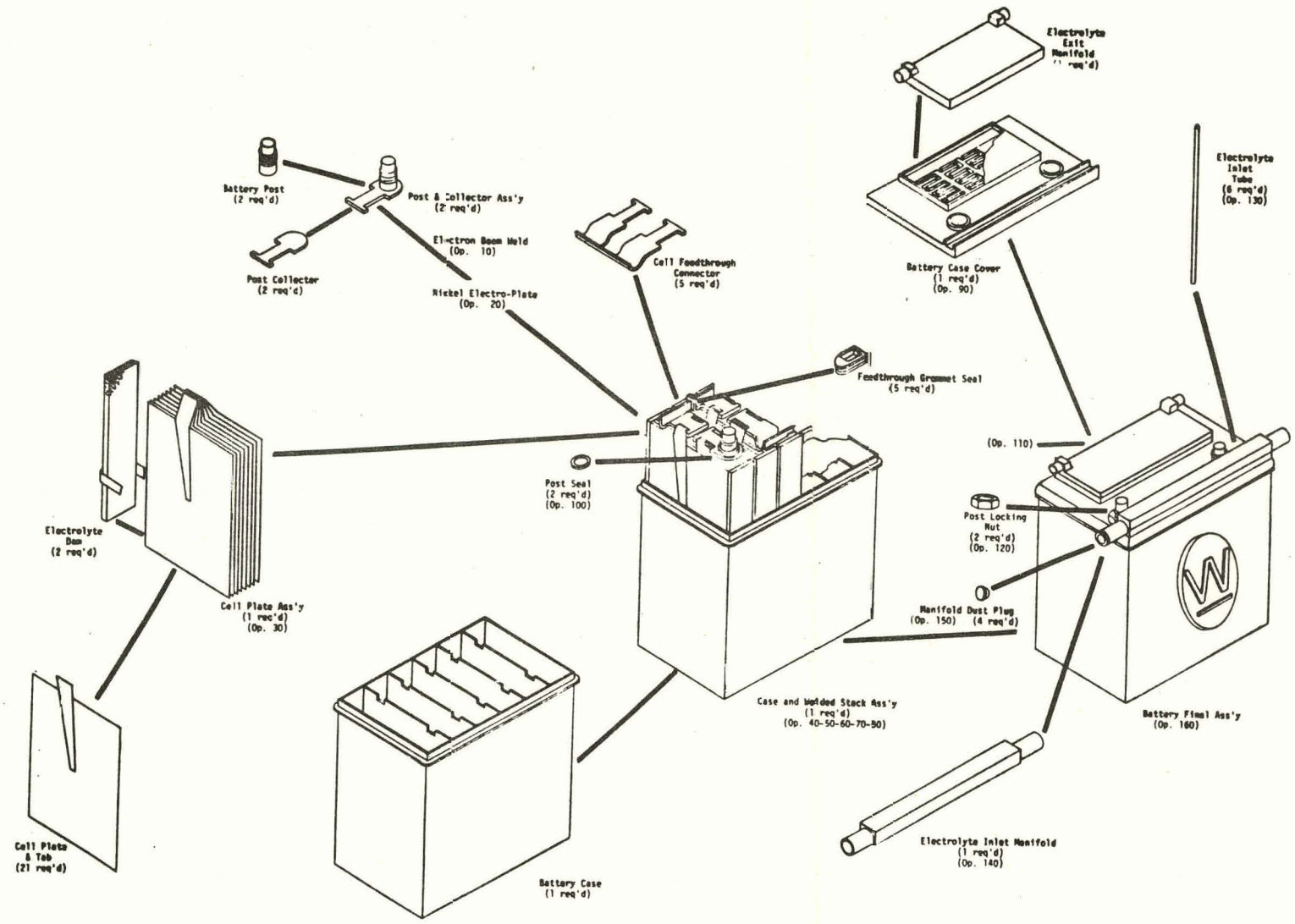

Figure 2.9. Six-Cell Module Design Concept

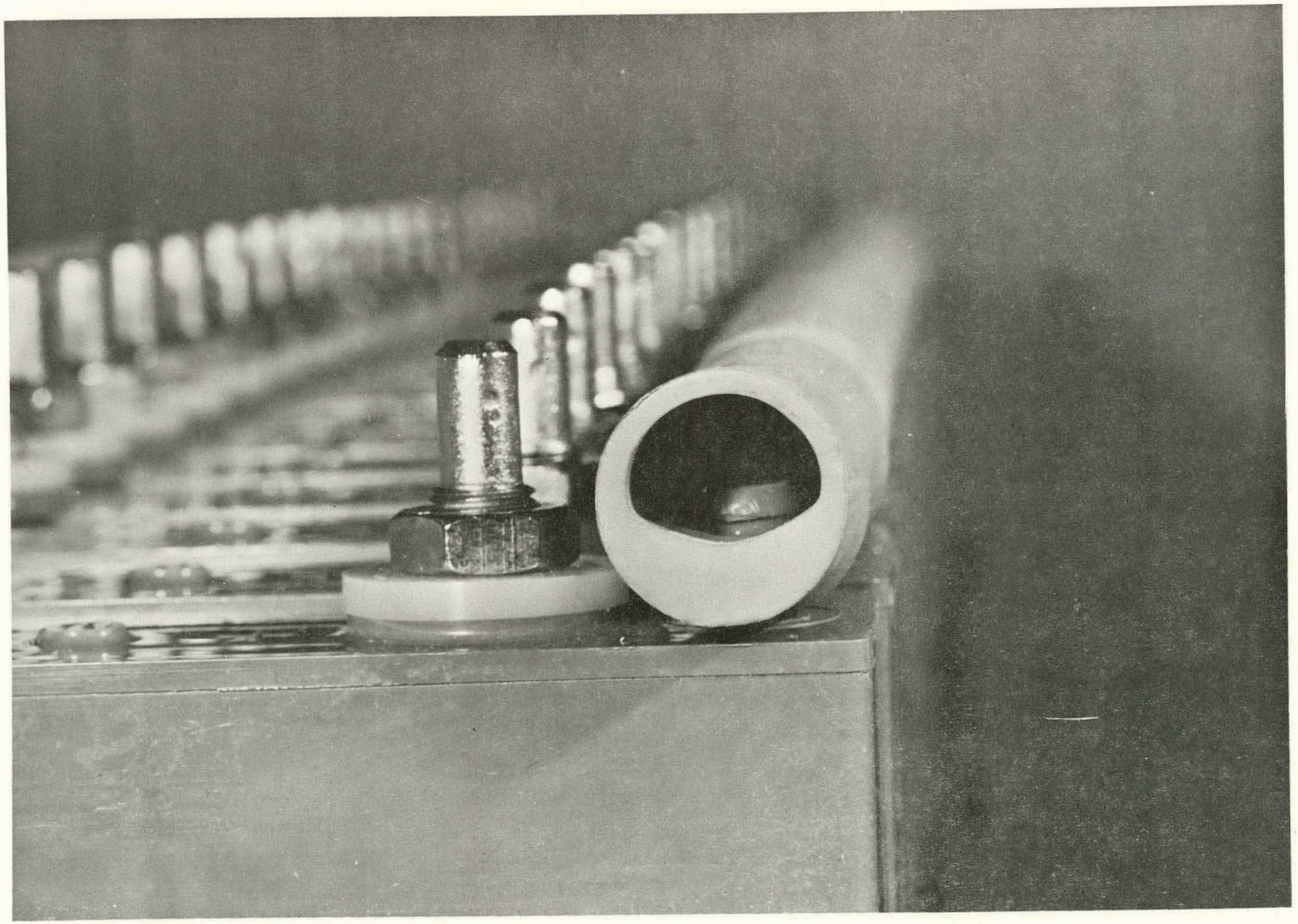

Figure 2.10. Twenty-One Cell String Manifold

improve design, (2) provide information of interest to potential users, who have a need to know many performance, environmental and safety aspects of the system.

For Task 2, the System Development portion of the contract, testing continues to concentrate in several areas. Prototype-size iron and nickel electrode tests are being performed to assist in evaluating design, materials and process changes and determining their effect(s) on improving performance. Also, full size nickel-iron cells are being tested in finished, molded containers. Six-cell modules, as used for the DOE/JPL "2 x 4" battery, are also being tested for performance and design evaluation. Testing of full size batteries is now part of the DOE/JPL program of near term electric vehicle evaluation. Two 90-cell batteries, including electrolyte management systems, have been supplied to JPL.

The testing is to provide, ultimately, information on the operational and performance characteristics in the following areas: (1) pretest, (2) charging and charge efficiency, (3) capacity, (4) power, (5) charge retention, (6) life, and (7) environmental aspects, as temperature.

Developmental cells and modules (and batteries) are tested with circulation of electrolyte during both charge and discharge. Up to five charge/discharge 80% DOD cycles can be run each day, with 20 full-size cell test positions available. Up to 25 full-size iron and/or nickel electrodes can also be tested at this same rate.

A special, variable depth-of-discharge test station was designed to simultaneously test up to three 6-cell, full-size modules. The system was chosen in an effort to cease the practice of testing cells at 100% DOD and to provide information on cells tested in a condition more closely approximating battery usage. These stations can assist in obtaining added depth-of-discharge and life data. The system is capable of cycling the modules at different DOD's and can also be used in temperature/life tests.

The 3-station, full-size module tester is shown in Fig. 2.11. Here 3 modules are shown under test, complete with the electrolyte circulation system. Controls and instrumentation are in the rack at the right and power supplies and the voltage recorder are in the rack to the left of the modules.

2.5 PILOT PLANT OPERATIONS

Pilot plant operations include all operations for plaque, nickel and iron electrodes, cell, module and battery fabrication.

Production in the pilot line facility proceeded in the past year to the extent that the cells required for the 2 JPL batteries, 2 additional ANL/NBTL test modules and full size experimental cells were fabricated. Pilot line equipment and operations are presently being transferred to the Westinghouse Advanced Energy Systems Division at Large, PA, where future cells and batteries will be manufactured.

2.5.1 GRID FABRICATION

Grid fabrication continued until the present shut-down with the only change implemented comprising needle-stitched steel wool as the feed-stock material in making the grids.

2.5.2 IRON ELECTRODE FABRICATION

From September 1979 through August 1980, 6,050 composite-type iron electrodes were fabricated and collated into 550 cell stacks. During this period, the basic raw material, Fisher I-116 red iron oxide, was successfully replaced with a low cost red iron oxide, prepared and supplied by the Pfizer Company.

The raw active material was loaded into the electrode plaque by means of the same process as used in the prior year, i.e., two facilities were used, one for each basic process step. In the loading step, the

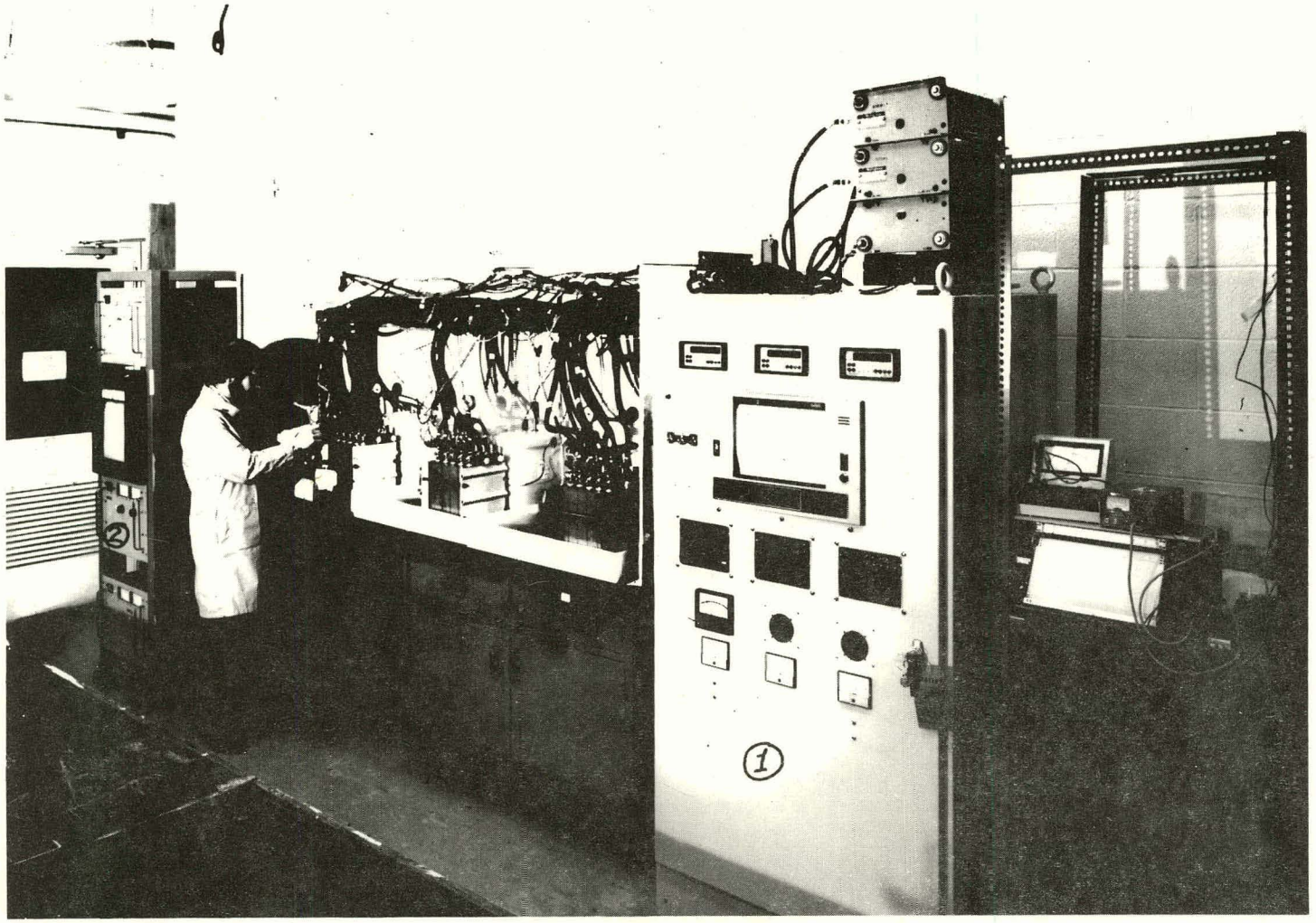

Figure 2.1[illegible]. Module Test Facility

plaque was purposely loaded with excess aqueous iron oxide paste. In the sizing step, controlled amount of the paste was retained in the plaque, by sizing it down to a predetermined thickness.

To lower labor costs and to reduce material waste, a design study was undertaken to combine the loading and sizing steps into one facility. The best approach was a system containing, in addition to the paste, a series of loading rolls, followed by a set of sizing rolls. As the plaque is propelled through the system, it is first loaded with excess paste and then sized-down, prior to it leaving the process line.

2.5.3 EPP NICKEL ELECTRODES

The electroprecipitation process (EPP) utilized for producing nickel electrodes is essentially as described in 2.1.2.4.

With respect to the nickel electrode fabrication, analytical data is gathered as part of Maxi-line plating and EPP solutions QA/QC. Other data, taken from QA/QC, include recording steel weight (grid plus tab), nickel plating weight, and thickness of the grids prior to EPP, as well as thickness and immersed electrode weights afterwards. Eight locations are consistently measured for the thickness determination. The weights taken prior to EPP and the immersed weight of the finished electrode permit a calculation of the active weights. Both quantities are significant for QA/QC means, and were determined for 10% of the electrodes in every run.

2.5.4 CELL ASSEMBLY

Changes in cell fabrication were discussed in Section 2.3. Cells assembled fall into one of the following groups: (1) developmental cells SCT vehicle contains two of these 21-cell strings, as well as one 18-cell string and two 15-cell strings (90 cells/battery), designed to fit into the SCT Rabbit battery compartment.

Six modules have been tested on the auto life cycler. An additional four modules were recently sent to the NBTL, two as part of this program and two as part of the JPL program.

2.5.5 BATTERY ASSEMBLY

Three hundred twenty-nine (329) cells have been fabricated for the JPL program to permit building and delivering the two full-size batteries and spare cells required. One battery system has been delivered; the other is presently on test at Westinghouse and scheduled for delivery in November, 1980.

Fig. 2.12 shows the present method of assembling full-size nickel-iron cells into strings. Strings of cells are designed in such a way as to efficiently use the particular vehicle battery compartment. In the figure, a 21-cell string is shown, complete with circulating system manifolding, end clamping plates and string binding. The first battery that has been constructed on the JPL/DOE program at Westinghouse for the SCT vehicle contains two of these 21-cell strings, as well as one 18-cell string and two 15-cell strings (90 cells/battery), designed to fit into the SCT Rabbit battery compartment.

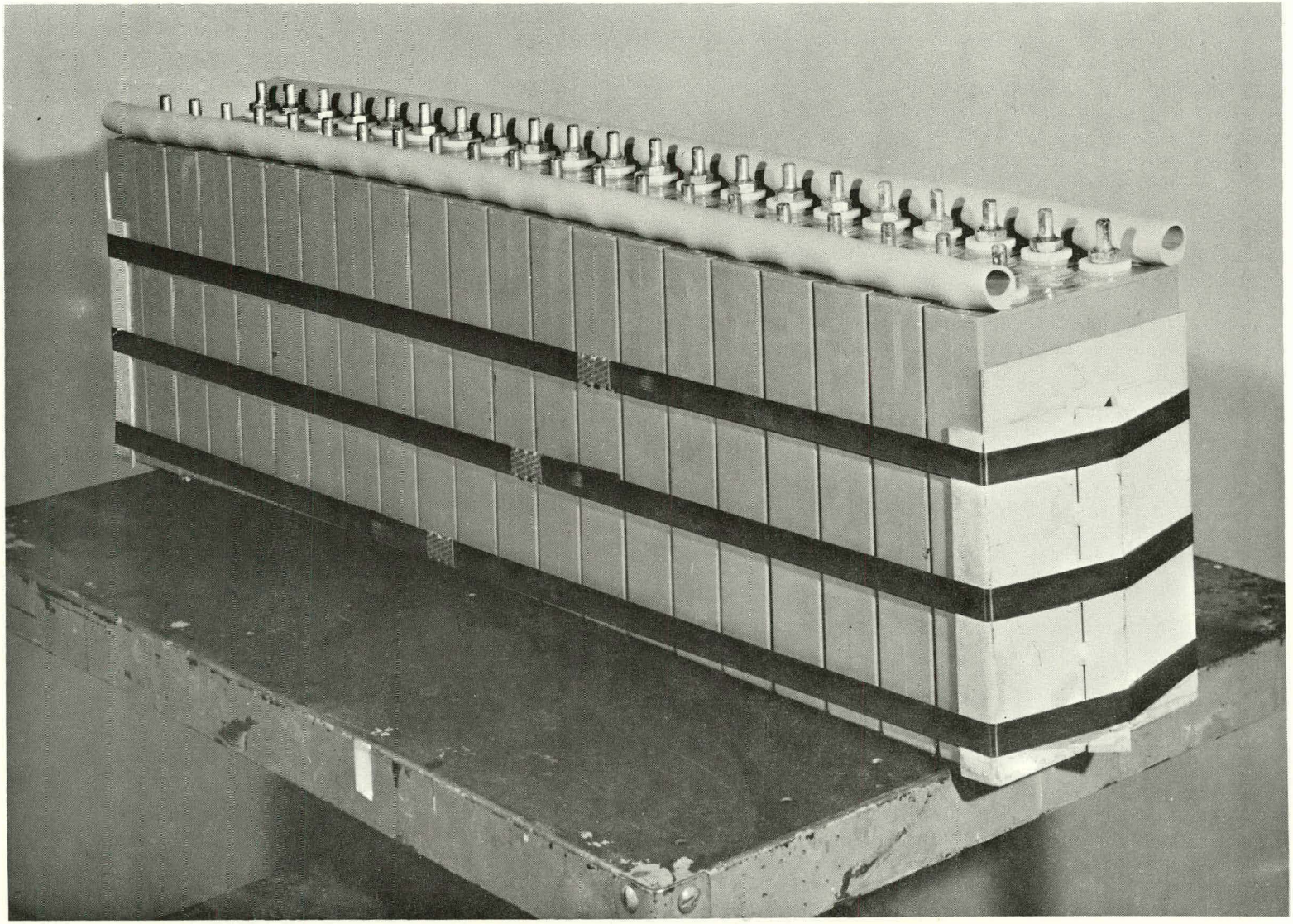

Figure 2.12 Twenty-One Cell String

3.0 TECHNICAL PERFORMANCE

Initial program goals and projected demonstration values are presented in Table 3.1. Full-size cells and three plate cells were initially cycled to 100% depth of discharge each cycle. These cycling tests were more stringent than those required for long life cycle testing, which are now conducted on cells in finished molded case/covers, to 80% depth of discharge, based on rated capacity. The cycle life test cells employ electrolyte circulation, electrolyte composition and temperature control, and minimization of $CO_3^{=}$ formation in the electrolyte. All these controls have been incorporated into the auto cycler, single cell test system and into the "closed," 3-module test system, which is used to test up to 6 cells/module. The cell test system operates with 20 test stations in the auto cycle life tester. Twenty-five 3-plate cells can be simultaneously tested.

Full-size cells have always been on test in containers of the proper volumetric constraints, as per design specifications. Cells made with molded cases and covers are being rated on performance, based on their actual weights, including electrolyte. Cells are being fabricated with cases and covers made of GE Noryl 225.

3.1 THREE-PLATE CELL TESTS

Full size electrodes are tested in a 3 plate cell configuration to provide initial performance evaluation of design and process configurations prior to full size cell evaluation. The following sub-sections summarize the results of this test program.

3.1.1 EPP NICKEL ELECTRODE TESTS

Table 3.2 summarizes 3-plate cell test results on EPP nickel electrodes. Electrodes comparable to state-of-the-art technology deliver 21 to 26 Ah, depending on EPP processing conditions. From 6 to 33% decline

TABLE 3.1

NICKEL-IRON BATTERY TECHNICAL GOALS

Characteristics	Preliminary Contract Goals (Set Dec. 1977)	Best Present Demonstration
1. Battery Capacity (kwh) (100% rated)	25	26.5
2. Battery Dimension m H	0.28	0.28
(m H x m W x m L) m W	0.38	0.38
m L	2.21	2.21
Volume (ℓ)	230	230
3. Weight (kg)	417	420
4. Volumetric Energy (Wh/ℓ)	100	143
5. Specific Energy (Wh/kg)	60	58[r]
6. Specific Power (W/kg)		
Peak Battery	100	175
Sustained @ C/3	20	--
7. Duty Cycle		
Charge (h)	4-8	C/3 for 4h
Discharge (h)	2-4	3
8. Lifetime		
Deep Discharges	2000	≈500
9. Price/Energy[c] ($/Kwh)	<60	--
10. Energy Efficiency (%)	>60	54

TABLE 3.2

EPP-TYPE NICKEL ELECTRODE 3-PLATE CELL TEST RESULTS

Plate Description	Initial Capacity[b] Ah	Initial Ah Eff., %[c]	Life Characteristics Cycles[d]	% Decline[e] Capacity	Remarks[a]
3E	15.4	-	50	20	Control, Pure $Ni(OH)_2$
11E	25.2	76	625	51	038CE Comparison Cell -- Cross-Fiber, Standard Density
27E	25.7	77	344	37	026CE Comparison -- 3.23 mm diameter holes
49E	19.7	59	248	32	#1 Fiber Plaque
1004E	21.8	66	560	59	Control for 1007
1005E	13.0	39	215	9	Manganese Dopant
1006E	15.8	48	208	15	Calcium Dopant
1007E	22.4	67	307	58	EPP Process Variation
1008E	14.0	42	300	0	Barium Dopant
1009E	15.5	47	59	12	Iron Dopant
1011E	17.8	54	200	17	Needle-Punched Fibers
1012E	14.8	45	120	0	High Fiber Density
1013E	20.3	66	350	39	068CE Comparison Cell
1025E			159		Brush Design Plate
1028E			184		Brush Design Plate
1048E	20.2	61	266	36	High Fiber Density
2114E	23.9	72	405	39	0.25CE Comparison Cell 3 channels, 3/0 steel wool

TABLE 3.2 (CONTINUED)

Plate Description	Initial Capacity[b] Ah	Initial Ah Eff., %[c]	Life Characteristics Cycles[d]	% Decline[e] Capacity	Remarks[a]
3183E	17.4	53	505	36	Barium Dopant
2558E	18.6		>212	9	083CE Comparison Cell Reactively Sintered
2650E	20.7		>149	4	092CE Comparison Reactively Sintered
2707E	18.7		>112	3	094CE Comparison Cell Sinter + Ni Replate
2801E	17.8		>112	6	Pure Nickel Fiber Control
2902E	25.7		> 25	2	Pure Nickel Fiber Control

a. Special feature, components, weight (kg) and volume (l).
b. C/3 discharge, 4-8 hour charge.
c. Based on at least 5 consecutive cycles.
d. "Greater than" symbols denote continuing operation.
e. Percent decline from initial.

in capacity is usually noted after 200-300 test cycles of standard technology plates (Table 3.2, annual report for FY '79). 11E and 1004E, driven to approximately 500 test cycles, further extends this capacity decline; showing 51% to 59% decline.

Tests to evaluate the merit of standard fiber thickness range against a more coarse (Electrode 49E) and finer (Electrodes 27E and 2114) fiber range did not reveal any effect of fiber size on rate of capacity decline. However, the 49E electrode test suggested that coarse fibers may not collect electrode current efficiently, resulting in a lower initial capacity for the electrode.

Experimental electrodes 1005E, 1006E, 1008E, 1009E, and 3183E represent the present state of EPP technology, with respect to the possibility of replacing cobalt active material dopant with more economical, alternate materials. As discussed in 2.1.2.1, it is still a moot question as to whether EPP methods can be adapted so that higher, and, therefore, more effective concentrations of these additives can be evaluated. The particular electrode tests do serve to show, however, that the low dopant levels obtained did serve to maintain the percent capacity decline within the range observed for cobalt-doped electrodes. Without any dopant whatsoever, pure $Ni(OH)_2$ active material declines to approximately 20% of its initial capacity value in 50 cycles (electrode 3E, the control sample). With the sole exception of iron, all dopant materials tested appear to remain candidates for future substitution of cobalt.

Electrodes employing higher - density fibers (1012E, 1013E, 1048E) did not show significant increase in cycle life, but did demonstrate more efficient use of active material. This change in electrode design demonstrated that some nickel could be removed and replaced with less expensive steel, yielding a potentially lower - cost electrode.

Treatment of the high density fibers in the reactive sintering process (2558E, 2650E) further improved the electrode design by producing

a stronger fiber plaque, showing less capacity decline while on cycle life. These two cells are continuing on test.

Electrode 2707E, although not very far in cycle test, shows that nickel replate over the reactively - sintered fibers does provide additional performance benefits. Judgement is reserved on the need for nickel replating, however, until this continuing test is completed.

Electrodes 2801E and 2902E are baseline cells employing pure nickel fiber current collectors, which will provide a comparison of the performance of nickel positive active material which is not affected by any possible iron contamination.

3.1.2 PASTED NICKEL ELECTRODE TESTS

Full-size pasted nickel electrodes (2.00 to 2.40 mm initial thickness) display 20 to 22 Ah capacity at the C/3 drain rate in the best 3- plate test cells to 1.0V cutoff voltage, versus iron counter electrodes. These electrodes were designed to investigate various active materials and paste formulations. Active materials under investigation include: ozonated nickel hydroxide slurry, commercially available green nickel hydroxide and nickel carbonate. These materials represent a departure from the thermal preparation procedure, previously used, since they are easier and less expensive to obtain in large quantities and show similar performance and life characteristics.

Tests on these electrodes which reflect continuing process and material improvements, are between 100 and 200 test cycles. Tests with ozonated nickel hydroxide and commercial green nickel hydroxide, both containing 5 W/o $Co(OH)_2$, are nearing 200 test cycles and are producing 21 Ah with little decline from their peak values. The ozonated material achieved maximum electrochemical capacity of 22 Ah in a few forming cycles, whereas electrodes made from commercial green nickel hydroxide required about 10 cycles to achieve a level output of 22 Ah. Testing of full-size electrodes, using nickel carbonate as the starting material are

in the early stages of cycling but show promise of achieving 23-25 Ah output at loadings comparable to the ozonated material or commercial nickel hydroxide.

3.1.3 BRIQUET IRON ELECTRODE TESTS

All effort on the briquet type iron electrode has been deferred to enable concentration on improving the composite electrode approach.

3.1.4 COMPOSITE IRON ELECTRODE TESTS

Results on full-size test electrodes have been summarized in Tables 2.1 and 2.2 of Section 2.2. The composite-type iron electrodes have demonstrated a stable capacity of 22-23 Ah at up to 1,000 test cycles to date at 80 and 100% depth of discharge cyclic life testing. This stability has been maintained in electrodes having variations in nickel plating, steel wool fiber type and phenolic content of the active material paste, suggesting none of these factors are critical to stable performance, in the ranges specified in Table 2.2. This improved performance has been attained in 1.00 mm thick electrodes. Some electrodes have tested to 1,150 cycles to date, delivering 18.0 Ah/plate at that test level in the 3-plate test. Nickel plating is not necessary on the iron electrode grid structure for long cycle life. Newer technology iron electrodes are approaching 600 test cycles with capacities at 25 Ah.

3.1.5 SUMMARY OF THREE-PLATE TEST RESULTS

EPP electrodes are wet and therefore cannot be accurately weighed for active material content. However, based on electrodes of 23 Ah capacity, performance of EPP electrodes is estimated at 0.26 Ah/g active material and 0.11 Ah/g total electrode weight (target performance is 0.25 Ah/g active and 0.14 Ah/g electrode). EPP nickel electrodes indicate ~6% loss in capacity in 300 test cycles in one of the better

electrodes. At up to 500 test cycles, a decline of up to 50% of the original capacity can occur in the unrestrained, 3-plate test.

Full-size, pasted nickel electrodes deliver 20 to 23 Ah for several hundred cycles, to date. These loadings are 90-105g active material in electrodes of 1.80 to 2.30 mm thickness (~.22 Ah/g active material).

With respect to individual electrode gravimetric performance goals, composite iron electrodes are approaching target performance (0.40 Ah/g active material and 0.27 Ah/g total electrode) at 0.40 Ah/g active and 0.25 Ah/g electrode, based on 29.0 Ah capacity obtained for the electrodes.

Work is continuing to improve the performance of nickel electrodes by modifications in electrode construction, active material formulation and processing.

3.2 FULL-SIZE CELL TESTS

Testing of all cells is done with electrolyte circulation for the 100% and 80% DOD test cycles. Based on a nominal capacity of 230 Ah, the cells have been charged at 83.3A/3.7h (300 Ah, in) and discharged at 83.3A/1.0V per 100% DOD cycle. For the 80% DOD cycle, the cells have been charged at 83.3A/2.9h (240 Ah, in) and discharged at 83.3A/2.2h (184 Ah, out).

Again, these tests use a circulated and temperature controlled electrolyte condition (30°C on charge and 40°C on discharge -- bulk electrolyte temperature). Occasionally all are given a full charge of 83.3A for 4 hours and discharged at 83.3A to 1.0V cutoff to establish total cell capacity.

3.2.1 FULL-SIZE CELL TEST RESULTS

Fig. 3.1 shows the appearance of the present full-size cell that is used to evaluate the in-house state-of-the-technology. The 21-plate

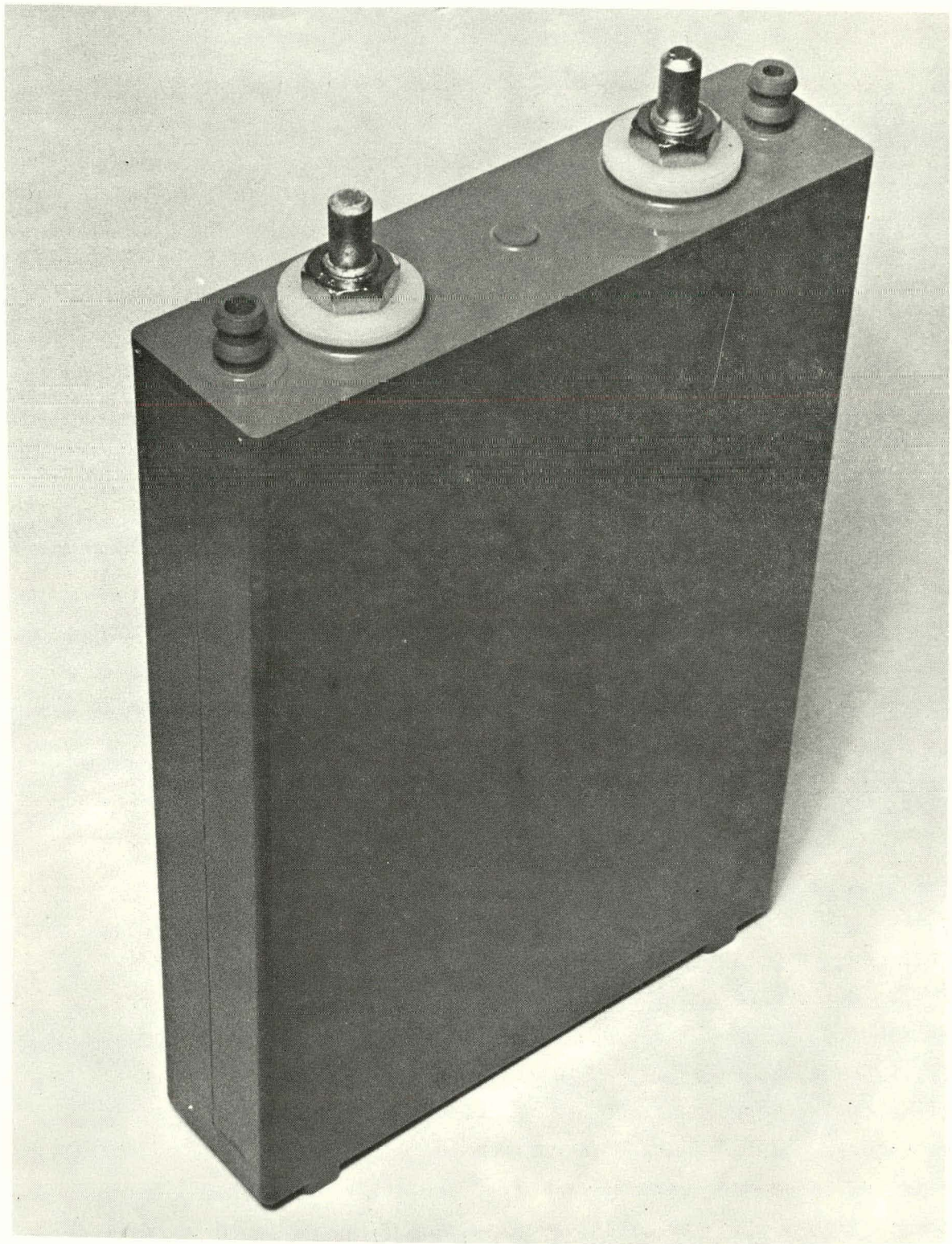

Figure 3.1. Nickel-Iron Cell Configuration

cell has barbed tube fittings, which secure the electrolyte circulation and exhaust gas manifolding (see Fig. 2.8), as part of the electrolyte circulation and gas venting system.

Table 3.3 presents the nature of some of the full-size experimental and/or pilot line nickel-iron cells tested, or on test, to date.

Couloumbic efficiencies have not been optimized in the test results reported in these tables, since the cells were cycled by in-house standard procedures, primarily to obtain the effects of variables in electrode and cell construction performance, as a function of cycling.

However, cell results have indicated the feasibility of attaining 50 to 60 Wh/Kg at the C/3 drain rate in full-size nickel-iron cells, having the design volumetric constraint and using EPP nickel and composite-type iron electrodes.

Cyclic life testing was modified to a mixture of 100% and 80% depth of discharge cycles at the C/3 drain rate and was further modified to permit electrolyte composition, circulation and temperature control.

Table 3.4 summarizes the best results obtained to date on full-size nickel-iron cells. Initial capacities of these cells ranged from 189 to 232 Ah at the C/3 drain rate. The better cells sustained up to 80% of their initial capacities after 325 cycles (Cell 128CE), 464 cycles (Cell 186CE) and 511 cycles (Cell 270CE). Maximum test cycles to date have been completed on Cells 169CE (556 cycles and 27% degradation), Cell 186CE (541 cycles and 24% degradation) and Cell 270CE (650 cycles and 28% degradation in capacity). Cell 194CE degraded only 9% in 355 test cycles, but was only 192 Ah, initially. Gravimetric energy density on these cells, based on an estimated 1086g contribution from electrolyte, case cover and terminals, ranged from 45 to 61 Wh/Kg at the C/3 drain rate for cells made with molded cases and covers. These cells ranged from 5.2 to 5.5 Kg per cells in total weight.

TABLE 3.3

CONSTRUCTION DETAILS OF FULL-SIZE NICKEL-IRON CELLS

Cell Code	Construction Details, Nickel Electrodes	Separator System Absorber, Barrier	Remarks
025CE	2.45 mm thick, EPP, coarse fiber, 3 vertical channels	SM 263.4, 3501	Rebuilt into new case and cover having electrolyte circulation capability. Unclamped and re-clamped at cycle 114.
048CE	2.44 mm thick, EPP, 2 vertical channels	KC 49696	50% >fiber density, 1/0 fiber
049CE	2.54 mm thick, EPP, 2 vertical channels	KC 49696	Special fiber
050CE	2.56 mm thick, EPP, 2 vertical channels	KC 49696	Barium-doped nickel electrodes
169CE	2.51 mm thick, EPP, 2 vertical channels	SM 263.4, 3501	Pilot line cell. Unclamped and reclamped at cycle 75.
186CE	EPP, 2 vertical channels	SM 263.4, 3501	Pilot line cell.
270CE	EPP, 2 vertical channels	SM 263.4, 3501	Pilot line cell.
194CE	EPP, 2 vertical channels	SM 263.4, 3501	Pilot line cell.
260CE	EPP, 2 vertical channels	SM 263.4, 3501	Pilot line cell.
056CE	2.64 mm thick, EPP, 2 vertical channels	K501	24g outer fiber layer.
057CE	2.44 mm thick, EPP, 2 vertical channels	K501	10g outer fiber layer.
060CE	1.78 mm thick, EPP, 2 vertical	K501	25-plate cell.

TABLE 3.3 (Continued)

Cell Code	Construction Details, Nickel Electrodes	Separator System Absorber, Barrier	Remarks
062CE	2.28 mm thick, EPP, 2 vertical channels	49696, 3501	Increased fiber density.
042CT	2.00 mm thick, thermal, 2 vertical channels	49696, 3501	Nickel plates bagged with separator, sealed onsides, bottom open.
061CE	2.28 mm thick, EPP, 2 vertical channels	49696, 3501	Increased fiber density.
063CE	EPP, 2 vertical channels	49696, 3501	Increased fiber density.
065CE	2.54 mm thick, EPP, 2 vertical channels	49696, 3501	
330CE	2.31 mm thick, EPP, 2 vertical channels	49696, 3501	Needle punched nickel plaques (from vendor)
331CE	2.31 mm thick, EPP, 2 vertical channels	49696, 3501	Needle punched nickel plaques (from vendor)
066CE	2.29 mm thick, EPP, 2 vertical channels	K501	Needle punched nickel plaques (from vendor).
067CE	2.43 mm thick, EPP, 2 vertical channels	K501	Higher fiber density
068CE	2.43 mm thick, EPP, 2 vertical channels	K501	Higher fiber density, needle-punched plaques (from vendor)
336CE	2.39 mm thick, EPP, 2 vertical channels	K501	Serpentine wrapped.

TABLE 3.3 (Continued)

Cell Code	Construction Details, Nickel Electrodes	Separator System Absorber, Barrier	Remarks
337CE	2.39 mm thick, EPP, 2 vertical channels	K501	19-plate stack (9 nickel electrodes)
338CE	2.56 mm thick, EPP, 2 vertical channels	K501	19-plate stack (9 nickel electrodes)
077CE	2.29 mm thick, EPP, 2 vertical channels	K501	50% >fiber density, needle-punched
079CE	2.29 mm thick, EPP, 2 vertical channels	K501	Barium substitution for cobalt
128CE	2.40 mm thick, EPP, 2 vertical channels	SM 263.4, 3501	Cells from Module 6-1, tested at ANL/MBTL for 327 cycles
080CE	2.50 mm thick, EPP, 2 channels	K501	Mini-line run nickels
081CE	2.41 mm thick, EPP, 2 channels	K501	Maxi-line run II
091CE	2.61 mm thick, EPP, 2 channels	K501	Mg-doped nickel active material
093CE	Four extra-height nickels, three extra-height irons	K501	Gas pressure relief design

TABLE 3.4

SUMMARY OF SOME OF THE BEST FULL-SIZE NICKEL-IRON CELLS TEST DATA

Cell No.	Initial Ah	Capacity Cycle	Best Wh/Kg	Cycles to ~80% of Initial Ah	Total Test Cycles	Total % Loss of Initial Ah
025CE	232	5	61	195(76%)	383	35
042CT	210	31	50	176(83%)	242	25
056CE	203	69	45	168(83%)	216	29
061CE	219	12	51	161(76%)	203	29
062CE	218	30	49	175(80%)	265	45
128CE	210	~10	--	325(79%)	357	21
169CE	225	5	49	233(77%)	556	27
186CE	189	5	--	464(80%)	541	24
194CE	192	5	--	--	355	9
270CE	232	25	50	511(80%)	650*	28
330CE	~190	5	54	--	310	--
331CE	230	5	--	--	306	--

*Still on test at >800 cycles

The module design of Fig. 2.9 should effect a decrease in average weight of 9% and 14% in volume. This would improve the gravimetric energy density per cell to 49 to 59 Wh/Kg for the test cells described.

Fig. 3.2 shows the life cycle history of Cell 270CE which remains on test after 800 test cycles. This cell suffered an irretrievable loss of 10Ah after a 2,000h open circuit stand at 410 test cycles. At cycle 650 the cell delivered 167Ah, at cycle 511 (including the 10Ah loss) the cell was still at 80% of its initial capacity. Figs. 3.3, 3.4, 3.5, 3.6 and 3.7 show the discharge characteristic of this cell at test cycles 52, 366, 510 and 659 (100% DOD) and cycle 304 (80% DOD). Good average discharge voltages are obtained on this cell, even after 659 cycles (1.21V). Fig. 3.8 shows the charge-discharge characteristic of nickel-iron pilot line cells to 1.0V and 0-8V cut off at the C/3 drain rate.

3.2.2 LOW TEMPERATURE TESTS

Low temperature tests were performed on five cells that were grouped into a module configuration. Each of the cells had been previously bench tested, individually, for three cycles, to determine their capacities, with 30°C circulation during charge and 40°C circulation during discharge. The first three cycles of the cells in the module configuration were run to confirm capacity, but with 30°C circulation during charge and no circulation during discharge. In these initial ambient temperature cycles, no open circuit time existed between charge and discharge. In the next three cycles, charging was performed in ambient conditions with 30°C circulation, the module was then cooled to -5°C (typically over a 14 hour period), placed into a 0°C water/ice bath, and discharged with no circulation. Three additional test cycles were then run under ambient conditions to confirm capacity. The electrolyte concentration was then increased and the module test schedule was repeated.

In analyzing the data, open circuit losses in the cells at -5°C were assumed to be one-half those at 25°C (this tended to make the

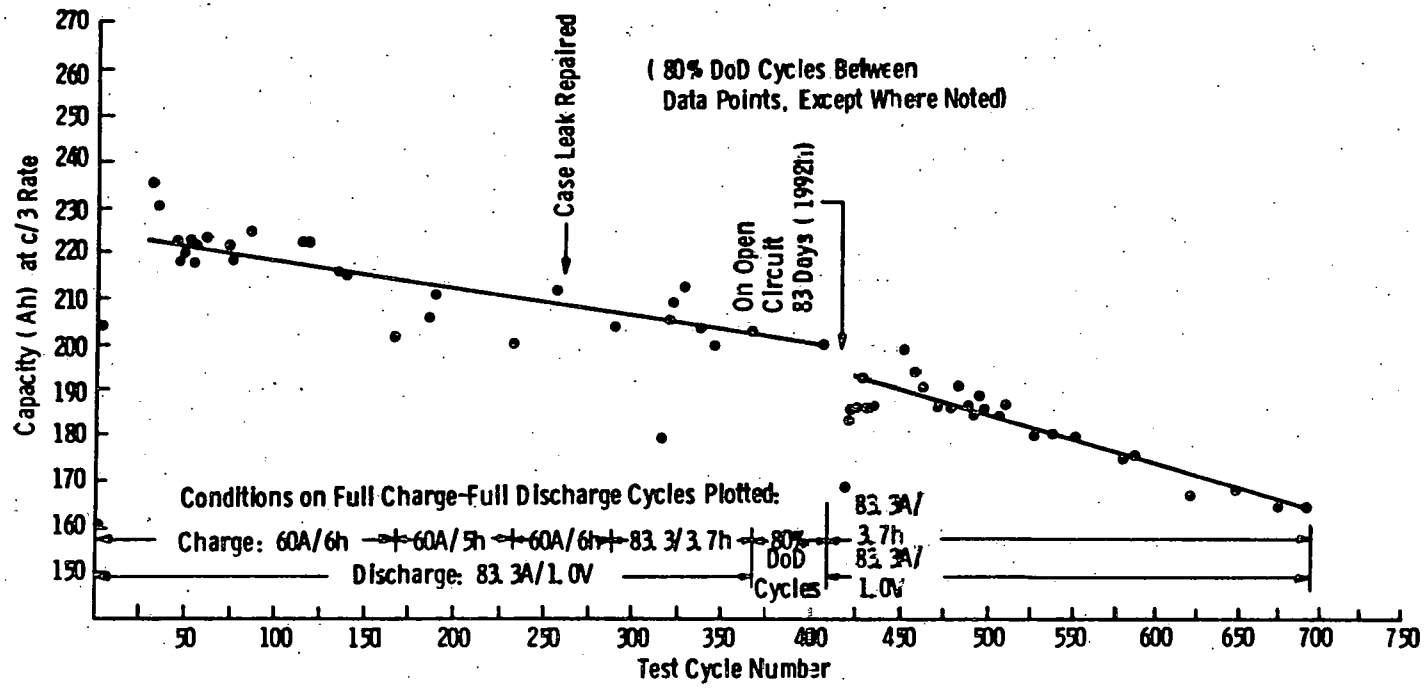

Figure 3.2. Cell 270CE Life Test Results

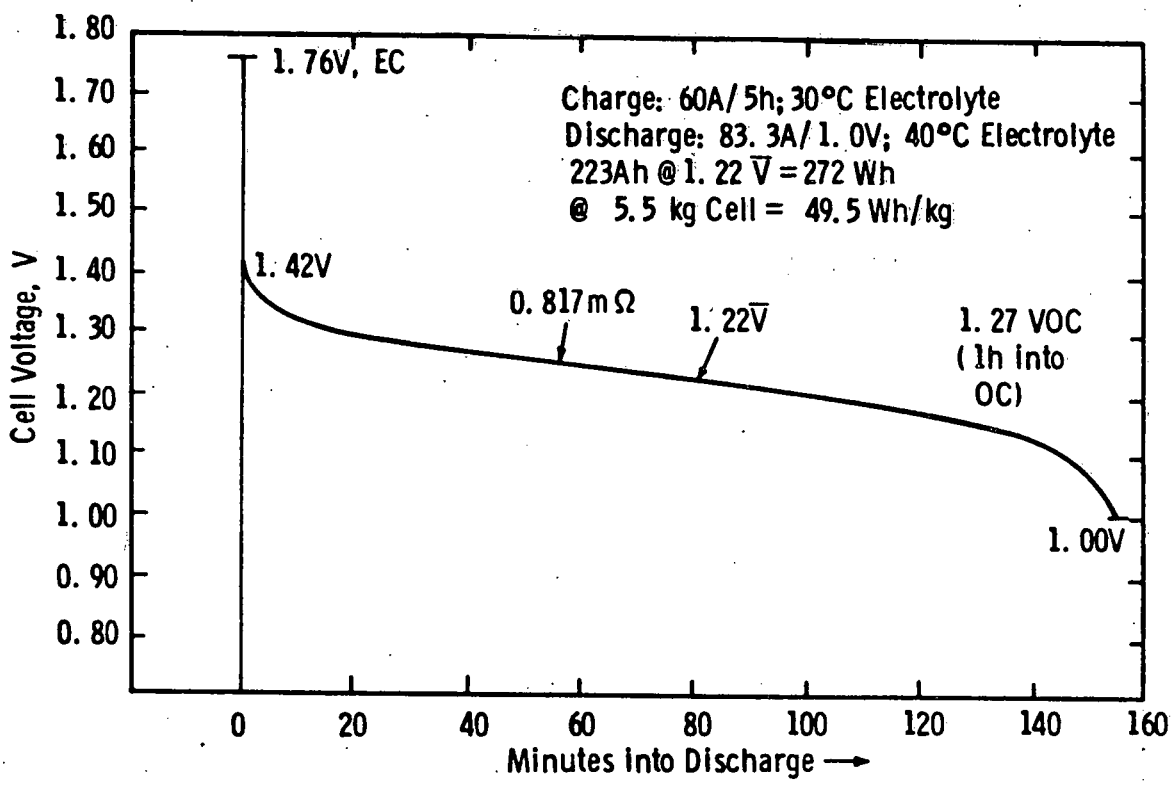

Figure 3.3. Cell 270CE Cycle 52 Full Discharge Curve

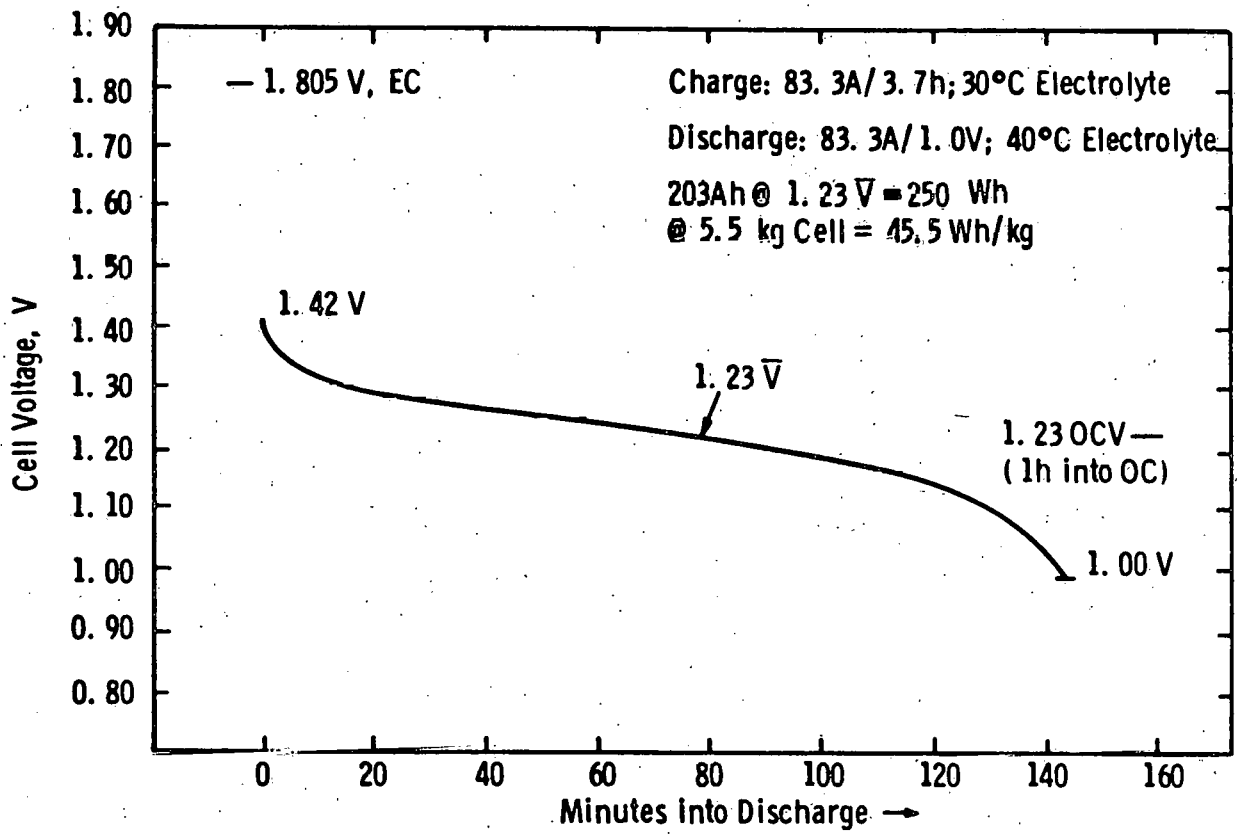

Figure 3.4. Cell 270CE Cycle 366 Full Discharge Curve

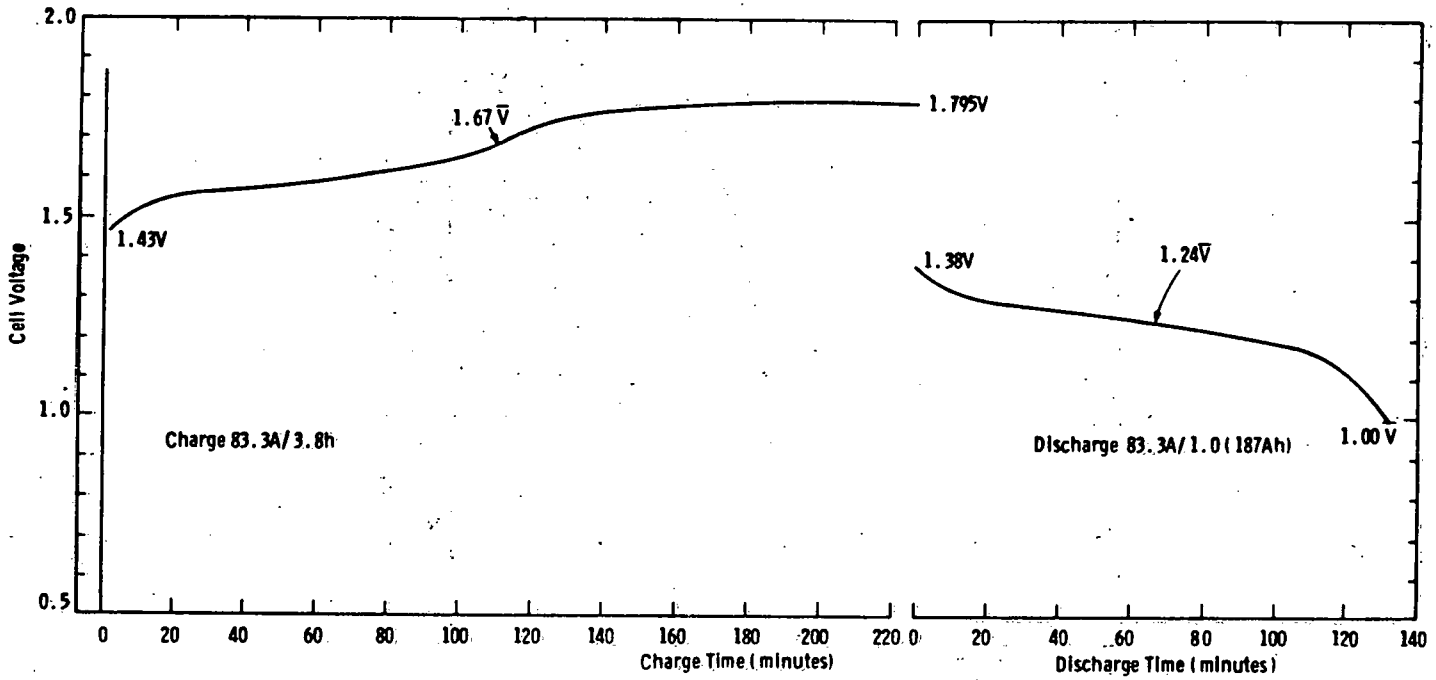

Figure 3.5. Cell 270CE Cycle 510 Full Discharge Curve

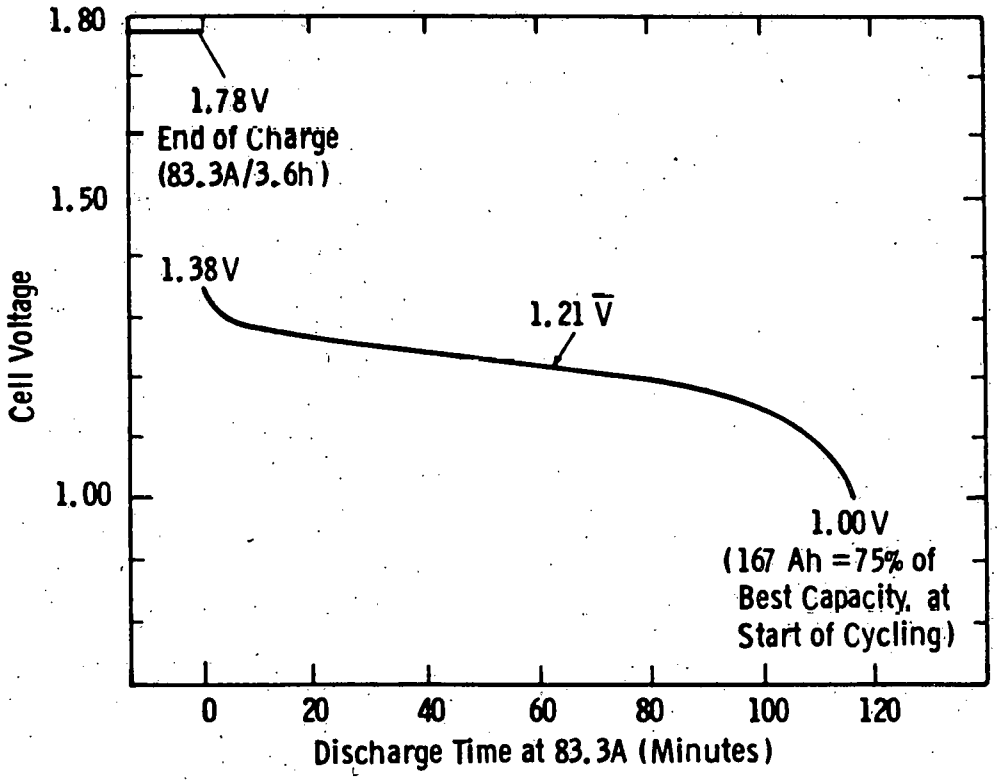

Figure 3.6. Cell 270CE Cycle 659 Full Discharge Curve

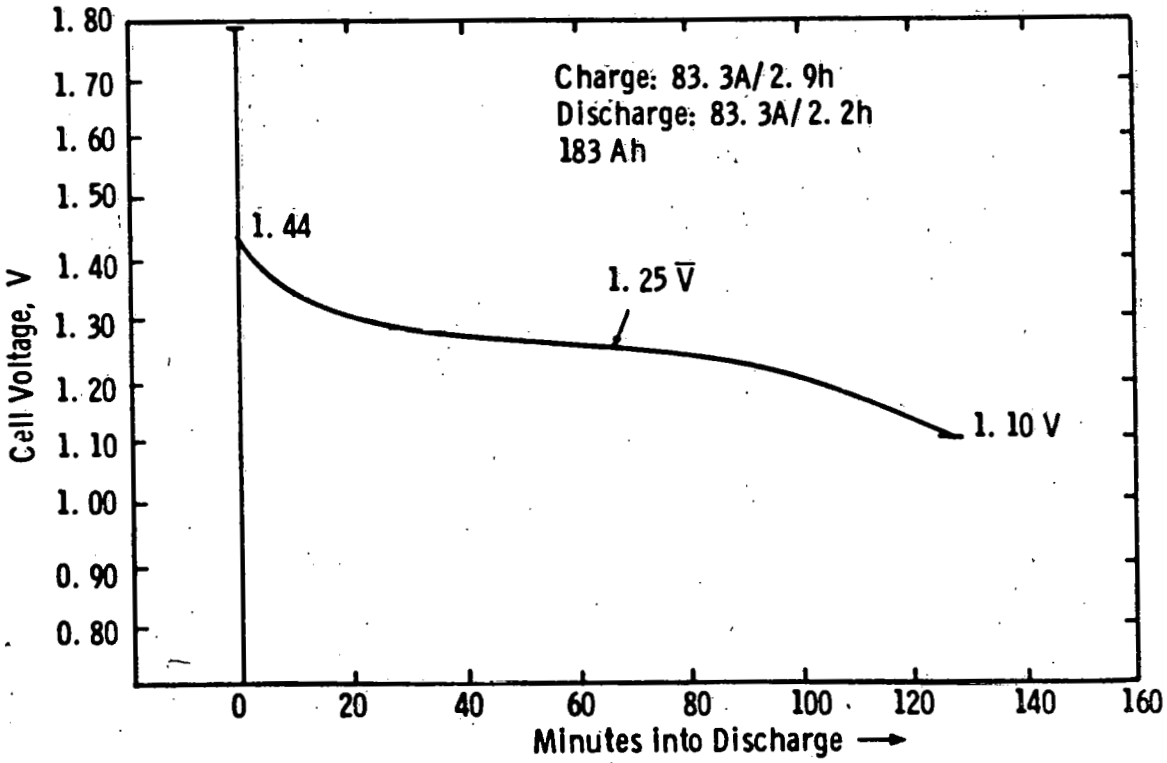

Figure 3.7. Cell 270CE Cycle 304 80% Depth of Discharge

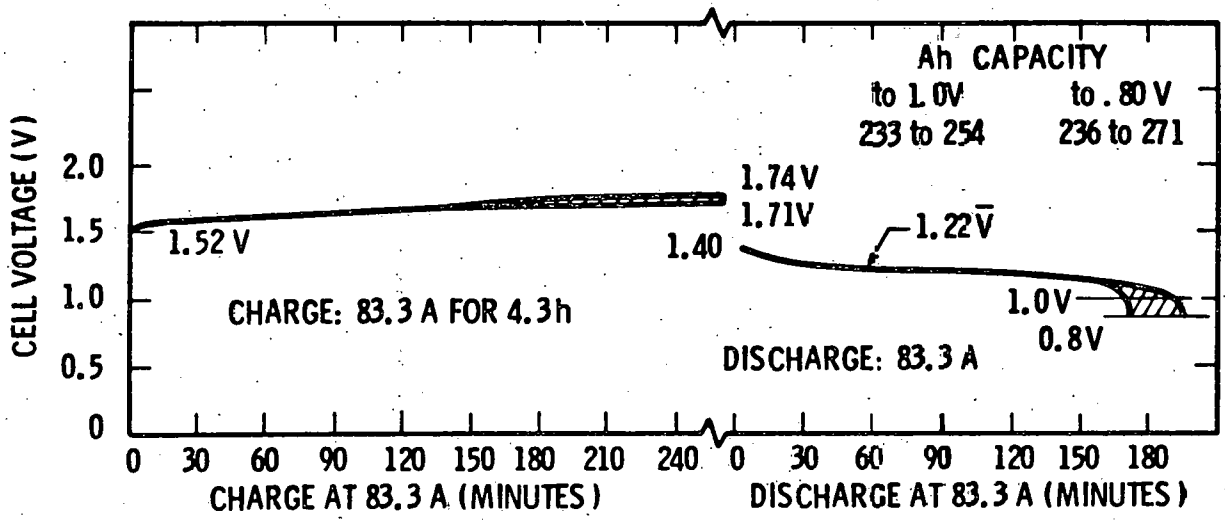

Figure 3.8. Voltage Characteristics of Pilot Line Cells

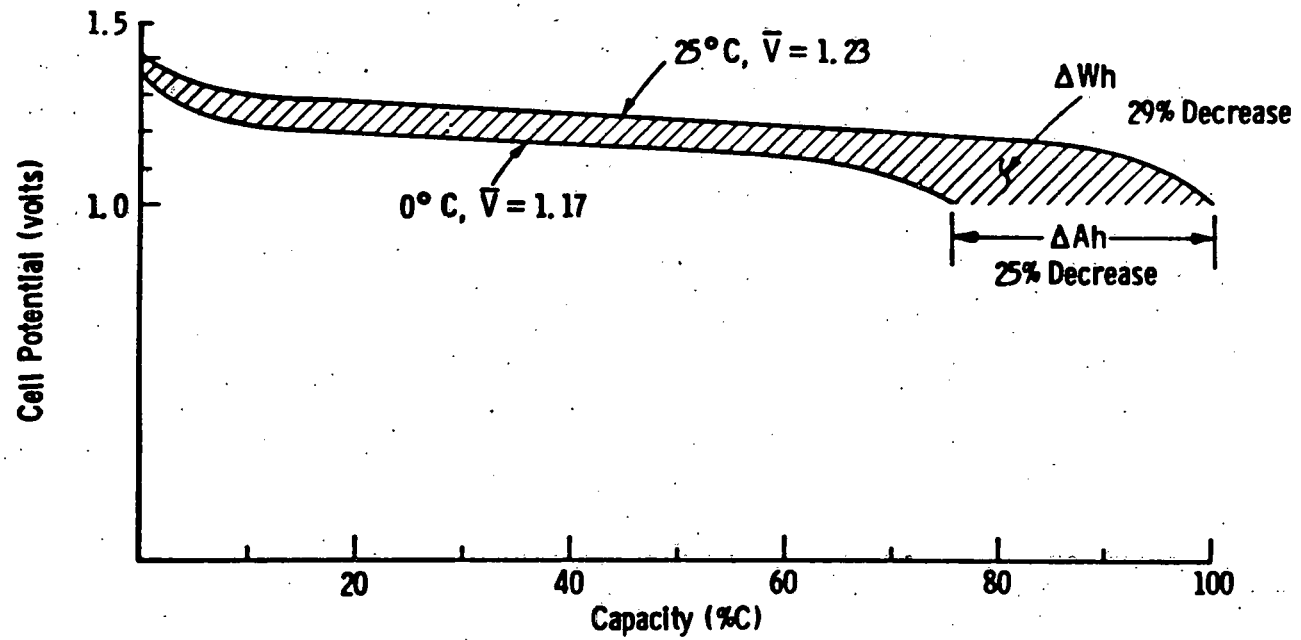

Figure 3.9. Low Temperature Performance

temperature effect seem greater). Figure 3.9 illustrates the effects. Average discharge potential dropped from 1.23V to 1.17V. Capacity at 0°C was still measured to 1.0V, where capacity losses ranged from 20 to 30%, with an average decrease of 25%. Energy loss averaged ~29% at 0°C, compared with 25°C. This performance is much better than predicted at the onset of the program, where up to 40% loss in capacity was expected at 0°C, when compared with room temperature capacity. Other recent cell tests show even better low temperature performance. Only 12% decrease in capacity at 0°C and 25% decrease at -17°C at the C/3 rate. At the C rate, a 22% decrease in capacity was observed at 0°C.

3.2.3 DISCUSSION OF RESULTS

Initial capacity performance of full-size cells is on target, with 230Ah per cell at the C/3 rate readily attainable within the cell design volumetric constraint. Gravimetric energy density of full-size cells having the design volumetric constraint, range from 49 to 61 Wh/Kg in finished cells, more typically, 50-54 Wh/Kg. This value can be improved ~10% with the concepted 6-cell monoblock design. Extended cyclic capability has also been demonstrated, with some cells operating 500 to 800 cycles to date. Low temperature ($0^{o}C$) performance has exceeded expectations. However, cyclic life test capacity stability is below expectations, with long-cycle test cells showing about 21% to 35% loss, based on initial capacity. The best cells have shown 20% loss in initial capacity at 464 cycles (Cell 186CE) and 511 cycles (Cell 270CE).

Several factors can contribute to nickel-iron cell capacity loss, during long time cycling 1) stack electrolyte starvation, 2) fiber metal grid corrosion, 3) internal gas pressure on charging, 4) deactivation and/or detachment of the active material, and, 5) excessive $CO_3^{=}$ pickup in the electrolyte.

Stack electrolyte starvation can be caused for several reasons. The first can be due to insufficient porosity in the electrode active

material, limiting wicking of electrolyte. This condition, in turn, can cause localized overheating on fast charge (as at the C/3 rate), with irreversible damage to active material and/or poor charge acceptance. Nickel electrode charge acceptance is best at ~35-45°C. Dimensional change, due to structural change in the active material during charge and discharge, results in swelling of the nickel electrode. This swelling can compress and reduce the wicking capability of the separator between the plates, causing localized dry out regions and, possibly, overheating of the active material on charge. It has been determined that a 42% volumetric increase is associated with the charge-to-discharge cation (K^+ and Li^+) movement -- in (charge) and out (discharge) of the active material and this, largely, contributes to the dimensional instability of the nickel electrode in the thickness direction. This swelling, as a function of charge-discharge cycling, is the most critical factor affecting performance and life of cells that contains nickel electrodes. Sintered nickel powder plaques have been developed and used for many years in the industry, (especially for nickel-cadmium batteries) to provide a rigid structure that will resist swelling, but, such structures are inherently expensive, when aimed at a selling price of $80/KWh (1980) in a nickel-iron battery. For this reason this solution to the nickel electrode swelling problem has been discounted for the Westinghouse program.

Loss of collector grid integrity can be another cause of capacity loss during cyclic life testing of nickel-iron cells. Increasing the mean fiber diameter, nickel plating at higher w/o pickup, relative to the grid, and reactively sintering the nickel electrode and replating with additional nickel are all potential solutions to this problem and are all being actively pursued. Cells with extreme cycling still have displayed nickel electrodes with good structural integrity (>300 cycles), so that grid collector failure does not seem to be a predominant factor, if any, in loss of capacity with cycling.

Deactivation of the nickel electrode active material can occur for several reasons. These include, physical detachment from the grid current collector, (by internal gas pressure and/or corrosion of the grid) thermal damage, dryout and, possibly, loss of water of hydration from the active material. These factors are best controlled by maintaining electrolyte availability, by controlled electrode porosity and electrolyte flow channel control. Thermal damage can be avoided by electrolyte availability during charge and discharge, electrolyte flow on charge, gas bubble release and back-wicking of electrolyte on discharge. Detachment of active material usually relates to fiber grid corrosion and/or mechanical breakdown of bonds between the fibers (usually a localized condition, only, but significant enough to show up in capacity loss in the electrode and cell).

Carbonate pickup in the electrolyte can occur if it is exposed to air and absorbs CO_2 from it. Maximum permissible concentration is about 50g/l K_2CO_3 in the electrolyte, at which level the electrolyte must be changed. At higher concentration, lower capacity and lower discharge voltage can result, probably due to carbonate having an adverse effect on the iron electrode. Carbonate pickup is avoided by operation in an essentially closed loop system. Gas produced during charge is vented through an isolating water bubbler, which also serves to shield the electrolyte reservoir from direct contact with the atmosphere. Therefore carbonate pickup should not be a major factor causing capacity loss.

In summary, the loss in cyclic capacity of the nickel-iron cells appears to be due, principally, to nickel electrode active material swelling, which is irreversible and can lead to electrode dryout, overheating on charge and permanent deactivation of active material in overheated regions. This problem is being addressed in several areas... optimization of pore volume/active material/grid volume, gassing control, strengthening the grid itself, utilization of grid designs aimed at

maintaining thickness integrity and utilization of a paste formulation nickel active material, whose density and chemistry may produce less overall electrode swelling.

3.2.4 CELL POST OPERATION EXAMINATION

Three modules from the first 2 x 4 battery were returned by JPL after 13 cycles because they had developed defective cells. Two cells appeared to have internal shorts and three had very high charge voltages. The three cells which had been observed to have high charge voltages (172CE, 219CE, 221CE) were found to have inlet tubes blocked with epoxy. Shorts were found in the other two cells (138CE, 146CE). Both shorts were at the top of a positive electrode. The separator, which had been accidentally folded down on assembly, left the top of the electrode bare, allowing the positive electrode to contact and short to the adjacent negative electrode. Conditions which caused these failures have been alleviated by changing the method of sealing inlet tubes and by using a serpentine wrap to assemble separators.

Fourteen experimental cells which had been cycled were dismantled when cycling was completed. Table 3.5 gives a summary of the construction, performance and final condition of these cells. Changes in cell construction, made as a result of these and other tests, are discussed in other sections of this report.

Module 6-1 was delivered to ANL/NBTL for testing in July 1979. Prior to shipment the capacity of the module was 239Ah to 6.0V at the C/3 rate. Cell 102CE failed at cycle 34 and cell 120CE failed at cycle 100. Each cell was bypassed when it failed so that cycling of the remaining cells could continue. Four cells were tested for a total of 327 cycles, when cell 107CE failed. Typical capacities obtained at NBTL were:

Cycle	Initial	150	200	250	300	327
Ah	215-220	180	172	165	157	161

TABLE 3.5

SUMMARY OF NICKEL-IRON CELL POST-OPERATION EXAMINATIONS

Cell No.	Construction	Max. Cycle	Capacity Ah	Final Cycle	Final Capacity Ah	Performance	Observations
017CE	Kendall SP126 absorber	32	254	90	121	58 cycles to 100% capacity	Separator & plates in good condition
022CE	0.635 cm holes in nickel plates	20	233	56	182	31 cycles to 100% capacity	Nickel plates expanded to 3.05 mm
023CE	High density steel fibers	49	242	76	147	15 cycles to 100% capacity	Nickel plate channels blocked
025CE	Finer gage steel fiber	25	262	383	153	Cell restraints loosened	Nickel plates expanded to 3.17 mm
026CE	Kimberly-Clark S 49023 absorber	8	250	84	105	18 cycles to 100% capacity	Nickel plates expanded to 3.05 mm
030CE	K-C 49696 absorber No barrier	48	224	48	224	All cycles to 100% capacity	Plate & separators in good condition
031CE	Celgard K-501 Separator	6	246	45	214	All cycles to 100% capacity	Nickel plates soft
032CE	K-C S49023 absorber No barrier	6	212	48	210	All cycles to 100% capacity	Nickel plates tough
038CE	Cross fiber nickels K-C S49033 absorber	2	214	23		All cycles to 100% capacity	Nickel plates expanded to 2.96 mm
042CT	Thermal nickel	25	225	246	137	Loosening cell restraints gave slight improvement	2% iron in nickel active material

TABLE 3.5 (CONTINUED)

Cell No.	Construction	Max. Cycle	Capacity Ah	Final Cycle	Final Capacity Ah	Performance	Observations
050CT	Barium in nickel active material	9	197	263	113	Cycled to 80% of rated capacity	Co in active material of one nickel plate
058CE	19 plates, K-C S 49696 absorber	31	212	130	131		Separators with black residue stuck to plates
060CE	Low porosity nickel plates	2	237	91	100	Low electrolyte flow	Plates and separators very dry
194CE	Celgard 3501 barrier Kendall 263.4 absorber	100	233	355	175	Cell case split on cycles 225, 348, 355	Plates and separators in good condition

The three cells 102CE, 120CE and 107CE failed because of shorts between adjoining plates. In cell 102CE the short was due to separator meltdown at the nickel tab region, during TIG welding of the electrode tab to the post comb. The short in cell 120CE, which occurred at the bottom of the stack, may have been caused by a sharp edge or fiber penetrating through the separator bag that sealed the iron plate.

A new method of fabricating the comb, using bar stock, helps prevent separator meltdown at the electrode tab region (see Section 2.1.3.2). Inspection of electrode edges before assembly insures that no fiber or sharp sheared edge protuberences exist to cause shorts. Serpentine separator wrapping (now being used) will avoid shorts caused by faulty bag sealing.

Table 3.6 summarizes procedures that are used in post operation examination of nickel-iron cells.

3.3 MODULE TEST RESULTS

Fig. 2.12 illustrates the module concept that is presently fabricated in the nickel-iron battery pilot line and that was used to construct the batteries this year. It differs from the module constructed and used to build the 2 x 4 battery (see Fig. 2.7 of the FY '79 Annual Report) for JPL in 1979. Principal construction changes include: location of manifolding at the outside edges of the cell; flexible rubber inlet and outlet manifolds, which seal onto barbed posts coming out of the cell cover; flexible intercell cables that are of the shortest length possible and that are mechanically clamped onto the all terminal posts.

Fig. 2.11 illustrates the 3 station nickel-iron module tester. Modules are tested with electrolyte circulation on charge and with or without electrolyte circulation on discharge. Testing temperatures are controlled to 30°C on charge and 40°C on discharge, via a cooling loop in the electrolyte reservoir. Tables 3.7 to 3.10 illustrate some module data obtained at the onset of testing. Excellent control performances

TABLE 3.6

POST-OPERATIONS ANALYSIS PROCEDURE FOR IRON-NICKEL CELLS IN MODULES

Step	Action
(1)	record open circuit voltage
(2)	record cell weight
(3)	cut cell from module with hacksaw, cut open top of manifolds and inspect inlet and outlet tubes
(4)	pour out and bottle electrolyte for analyses, if desired
(5)	cut off case bottom with hacksaw, examine bottom of stack and channel openings, examine case bottom for sediment
(6)	cut off cell cover at joint with hacksaw
(7)	unbolt terminals and remove cover
(8)	examine tubes, separator posts/comb welds
(9)	cut off posts with hacksaw, directly below comb-visually inspect welds
(10)	cut off case body from stack with hacksaw, by cutting at one vertical edge where the most stack to case clearance exists--carefully pry off case from stack
(11)	cut stack binding tapes
(12)	carefully remove electrodes, checking separator external condition
(13)	inspect unbagged nickels, remove bags from outside and central iron and inspect
(14)	measure outer and centrally-located nickel and iron electrodes for thicknesses at corners and between flow channels
(15)	inspect separator layers removed from outer and central iron electrodes for appearance, dryness, overheating, sticking, strength
(16)	store iron and nickel electrodes in separate trays of electrolyte of the same composition as in the test reservoir

TABLE 3.6 (Continued)

Step	Action
(17)	if electrodes are to be post tested for performance, allow excess electrolyte to drip off and seal in plastic bags until ready for 3-plate test assembly
(18)	depending on observations, chemical and metallographic procedures may be used to evaluate electrolyte active material for clues to explain observed behavior of module; electrodes should be bagged if long storage periods (>1 day) are anticipated, prior to analyses
(19)	if iron electrodes are to be discarded, they should be allowed to completely oxidize, first in a hood, in a vertical position resting in a tray having 1/2" of water as a heat sink, at least a week, or until it is obvious they have oxidized; allow bottom part to oxidize during this period by inverting the plates

TABLE 3.7

MODULE NO. 6-18 TEST DATA

Cell No.	Pressure (psi)	R_i (mΩ)	V_∞	Avg. Form Bench Cap. (Ah)	Cell Voltage at End of Discharge Cycle No. 1	2	3
398		.81	1.22	236	.99	.94	
441	2.0	.79	1.24	210	.94	.83	
442	1.5	.74	1.22	212	1.11	1.06	
444	1.2	.91	1.24	208	1.11	.92	
+449	1.5	.86	1.27	200	.95	-.13	
453	1.0	.99	1.26	205	1.10	1.02	

Module Capacity at cut-off (Ah)	246	247	
Module Voltage at cut-off	-	-	
Charge Temperature Range (inlet) °F	80-85	85	
Charge Temperature Range (outlet) °F	80-85	85	
Discharge Temperature Range (inlet) °F	85-120	125	
Discharge Temperature Range (outlet) °F	85-120	125	

+ removed before shipment to ANL, as a 5-cell module

TABLE 3.8

MODULE NO. 6-19 TEST DATA

Cell No.	Pressure (psi)	R_i (mΩ)	V_α	Avg. Form Bench Cap. (Ah)	Cell Voltage at End Δ of Discharge Cycle No. 1	2	3
504	2.2	.62	1.22	225	232*		
509	1.0	.61	1.23	219	255		
507	<1.0	.60	1.23	219	258		
+508	1.5	.58	1.21	212	244		
510	<1.0	.58	1.24	223	249		
511	<1.0	.59	1.24	212	249		

Module Capacity at cut-off (Ah)			
Module Voltage at cut-off	6.0		
Charge Temperature Range (inlet) °F	86		
Charge Temperature Range (outlet) °F	86		
Discharge Temperature Range (inlet) °F	104		
Discharge Temperature Range (outlet) °F	104		

+ removed before shipment to ANL, as a 5-cell module

- Testing: Chg. 70 A-6h
  Dschg. 70 A to 1.0_{CO}

* Cell #504 had 5h Chg.
Δ Ah capacity to 1.0V

TABLE 3.9

MODULE NO. NIPAK #5 TEST DATA

Cell No.	Pressure (psi)	R_i (mΩ)	V_α	Avg. Form Bench Cap. (Ah)	Cell Voltage at End of Discharge, Cycle No. 1	2	3
450	<1.0	.72	1.274	212	1.04	1.05	
452	1.0	.76	1.254	208	1.04	.98	
456	<1.0	.74	1.266	212	1.05	1.03	
459	2.0	.78	1.252	223	1.07	1.07	
462	1.0	.98	1.218	223	1.00	1.00	
465	1.0	.87	1.243	221	1.08	1.09	

Module Capacity at cut-off (Ah)	238	246	
Module Voltage at cut-off	-	-	
Charge Temperature Range (inlet)	85	85	
Charge Temperature Range (outlet)	85	85	
Discharge Temperature Range (inlet)	85	125	
Discharge Temperature Range (outlet)	85	125	

TABLE 3.10

MODULE NO. NIPAK #7 TEST DATA

Cell No.	Pressure (psi)	R_i (mΩ)	V_α	Avg. Form Bench Cap. (Ah)	Cell Voltage at End of Discharge Cycle No. 1	2	3
457	<1.0	.68	1.217	208	1.05	1.01	.75
470	1.5	.71	1.217	208	.96	1.01	.99
472	1.0	.78	1.229	217	1.06	1.00	1.06
473	<1.0	.99	1.204	196	.98	1.00	.97
474*	1.0	.69	1.257	187	.74	.78	
476	1.5	.68	1.227	210	.95	.97	.95
486	1.0						.95

Module Capacity at cut-off (Ah)	238	246	247
Module Voltage at cut off	-	-	-
Charge Temperature Range (inlet) °F	85	85	85
Charge Temperature Range (outlet) °F	85	85	85
Discharge Temperature Range (inlet) °F	85	125	125
Discharge Temperature Range (outlet) °F	85	125	125

*Replaced w/cell no. 486 after cycle 2.

were obtained in the cells comprising these modules -- 238-247Ah. Some cycles data on 2 modules are presented in Table 3.11 at 87 and 160 test cycles. Both of these modules (NIPAK 3 and 5-9, respectively) exhibited stable performance. However, both modules degraded in capacity with further cycling.

The best nickel-iron module data is still represented by Module 6-1, which was tested at Argonne National Laboratories, National Battery Test Laboratory. This module was tested for 327 cycles at which time it had degraded about 26% from its initial capacity. Other modules in test at Westinghouse have delivered 53 Wh/kg and 106-113 Wh/l based on a C/3 drain rate.

3.4 BATTERY TEST RESULTS

Two 90-cell batteries have been constructed and tested, as part of the JPL/DOE near-term electric vehicle test program. Tables 3.12, 3.13 and 3.14 summarize the data obtained for the 90-cell batteries.

Battery #1 strings (comprised of 2-15, 1-18 and 2-21 series connected cells) initially developed from 232 to 262Ah at a 70A drain rate (see Table 3.12). When these strings were assembled into the battery configuration, complete with circulating electrolyte systems (to fit into a South Coast Technology converted VW Rabbit hatchback), Battery #1 delivered up to 236Ah at the fourth test cycle (see Table 3.13). Battery #2 delivered 236Ah at the 70A drain rate and 204Ah when the drain rate was increased (from 70A to 104 to 135A see Table 3.14).

Table 3.15 summarizes and compares data obtained on the JPL " 2 x 4" battery, delivered by Westinghouse in 1979, and the 2 current JPL batteries.

Total battery energy of the two JPL batteries had increased to 25.9 KWh, from 22.7 KWh for the 2 x 4 battery. Also, energy density of the #1 JPL battery had increased from 46 (2 x 4 battery) to 53 Wh/kg at

TABLE 3.11

NICLEL-IRON MODULE CYCLIC TEST RESULTS

Charge 83.3A/3.9h
Discharge 83.3A/1.0V/cell

	NIPAK #3	Cycle 60 Ah		Cycle 87 Ah
Cell #	390CE	207		207
	391CE	190		187
	392CE	212		210
	394CE	210		208
	395CE	214		210
	396CE	209		204

	5-9	Cycle 153 Ah		Cycle 160 Ah
Cell #	243CE	196		197
	272CE	185		188
	201CE	183		181
	232CE	178		179
	197CE	186		187

TABLE 3.12

DOE/JPL BATTERY NO. 1, STRING TEST RESULTS

BATTERY CELL STRING DATA

		CHARGE				DISCHARGE			
STRING	CYCLE	AMPS	AH	T_S(°F)	T_F(°F)	AMPS	AH	T_S(°F)	T_F(°F)
15-1	1	70	350		80	70	252	80	122
15-1	2	70	350		NA	70	253	NA	NA
15-2	1	70	350		80	70	232	80	85
15-2	2	70	350		83	70	250	83	134
15-2	3	70	350		83	70	234	83	123
18-1	1	70	350		80	70	252	80	121
18-1	2	70	350		85	70	252	85	119
21-1	1	70	350		80	70	257	80	125
21-1	2	70	350		80	70	256	80	130
21-2	1	70	350		80	70	262	80	125
21-2	2	70	350		76	70	259	76	115

WEIGHT SUMMARY

STRING #	CELL WTS. (KG)	TOTAL STRING WTS. (KG)
15-1	78.6	81.5
15-2	77.5	80.4
18-1	95.7	98.9
21-1	110.7	114.4
21.2	110.8	114.5

TABLE 3.13

DOE/JPL BATTERY NO. 1, TEST CYCLE SUMMARY

		CHARGE				DISCHARGE				
DATE	CYCLE	AMPS	AH	T_S(°F)	T_F(°F)	AMPS	AH	T_S(°F)	T_F(°F)	COMMENTS
6/10/80	1	62/44	337	75	85	70	212	85	125	BENCH TEST
6/11/80	2	70	350	85	85	70	212	85	125	BENCH TEST
6/13/80	3	70	350	NA	NA	70	231	NA	NA	BENCH TEST
6/23/80	4	70	350	80	80	70	236	80	125	BENCH TEST

TABLE 3.14

DOE/JPL BATTERY NO. 2, TEST CYCLE SUMMARY

		CHARGE				DISCHARGE				
DATE	CYCLE	AMPS	AH	T_S(°F)	T_F(°F)	AMPS	AH	T_S(°F)	T_F(°F)	COMMENTS
9/16/80	1	70	350	80	85	70	186	80	125	BENCH TEST
9/17/80	2	70	350	85	85	70	236	85	130	BENCH TEST
9/19/80	3	70	350	80	80	65-270	224	80	130	BENCH POWER TEST
9/23/80	4	70	350	80	80	104-135	204	80	135	BENCH TEST

TABLE 3.15

WESTINGHOUSE NICKEL-IRON BATTERY CHARACTERISTICS

(DATA OBTAINED AT C/3 RATE)

	2X4	#1 JPL	#2 JPL
CELLS	90	90	90
WEIGHT, KG	492	490	N.A.
CIRCULATING SYSTEM	YES	YES	YES
DISCHARGE V	113	110	110
CAPACITY, AH	199	212-236	204-236
KWH	22.7	25.9	25.9
WH/KG	46.1	53.0	N.A.
WH/ℓ	104	106	106
VOLTAGE EFFICIENCY, %	78	75	75
COULOMBIC EFFICIENCY, %	69	68	69
ENERGY EFFICIENCY, WH	55	51	52

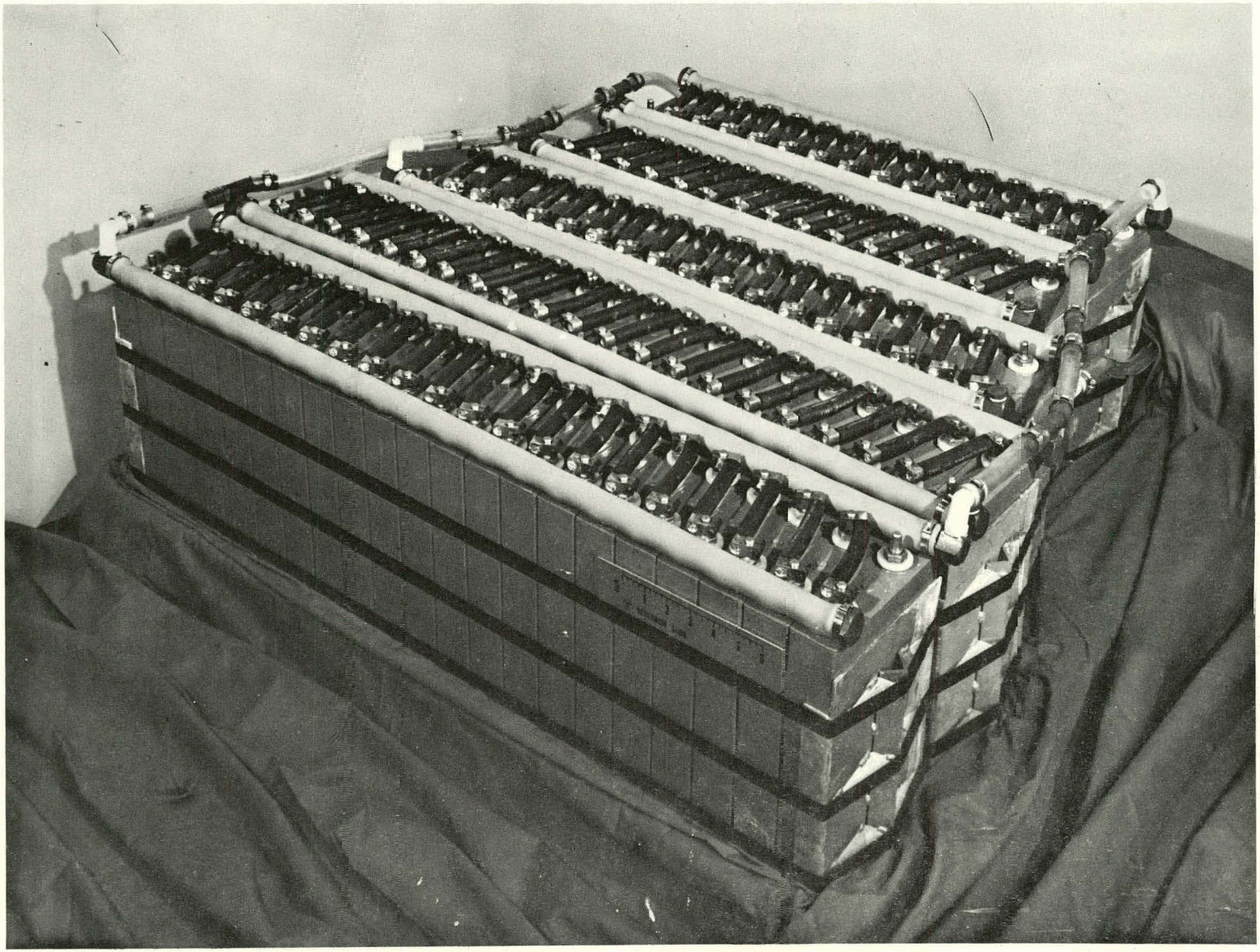

FIGURE 3.10. DOE/JPL 25 kWh Battery

the C/3 rate. No attempt was made to increase overall energy efficiency of these batteries, which were ~52% for the 2-JPL batteries, for a 50% overcharge regime. Fig. 3.10 shows the #1 JPL battery.

The #1 JPL battery was delivered to JPL in June 1980, and is undergoing testing there at the present time.

4.0 FUTURE WORK

The development program for FY '81 will be concentrated in three key areas:

1. Continue nickel electrode development to assess alternative grid structures and demonstrate paste loading process techniques.
2. Continue performance tests to demonstrate cycle life.
3. Conduct post operational analysis of failed cells and provide feed-back for electrode/component modifications.

The proposed task milestones are shown in Fig. 4.1.

4.1 NICKEL ELECTRODE DEVELOPMENT

The basic task objectives are the continued development and evaluation of nickel electrode designs and manufacturing processes conducive to meeting the cost objectives for large scale manufacturing.

Development and evaluation of alternative grid structures for EPP processes will be conducted with primary emphasis on minimization of electrode cyclic swelling. Optimization of active material to grid ratios will continue, to enable achievement of 0.15 Ah/g total electrode and stable capacity for 1,000 cycles.

Evaluation of low temperature chemical processes to manufacture active material for use in pasted electrodes with a goal of producing materials at costs lower than commercially available compounds will continue. An evaluation of additives to enhance active material utilization and cyclic stability will be completed.

Paste loading process development by impregnating sintered steel fiber metal grids with suitable commercially available active materials

Nickel Electrode Development	
Assess Alternate Grids	
• Demonstrate Alternate Low Cost Grids	7-30-81
• Select Optimal Grid/Active Mtl. Ratio	6-30-81
Pasted Active Material Dev.	
• Demonstrate Low Temperature Process	3-31-81
• Test Material in Full Size Cells	4-30-81
Paste Load Process Development	
• Scaled Process and Cost Analysis	6-30-81
Test and Analysis	
Performance Evaluation	
• Define Optimum Charge of Efficiency Conditions	7-31-81
• Define Control Parameters for Charger	7-31-81
Pilot Plant Operations	
Program Support	
• Fabricate Four 5 Cell Modules	Quarterly
• Revise QA Plan	12-30-80
• Update Process Specs	2-1-80
Program Management	
• Draft FY '81 Report	8-30-81
• Updated Commercialization Plan	5-30-81
• Updated Program Management Plan	2-15-81

Figure 4.1. FY '81 Proposed Task Milestones

will continue. A scale-up of the process for pilot production and identification of equipment and facilities requirements will be provided.

A nickel electrode manufacturing cost analysis for a pasted pilot process and comparison to the EPP process will be conducted.

4.2 TEST AND ANALYSIS

Life-cycle testing of electrodes, cells and modules to assess performance and demonstrate capability of cell designs to meet energy density, power life, and cost objectives will continue.

Tests will be conducted to optimize charge efficiency. These will include evaluations of constant potential, modified constant potential and other techniques amenable to minimizing charge energy input. Control parameters for charger design will be determined.

Post-operational analysis of cycled cells will be conducted to provide feedback for electrode/component design modifications.

4.3 PILOT PLANT OPERATIONS

Four 5-cell modules will be fabricated per quarter, incorporating the most recent development items. Up to two of these modules will be submitted to ANL/NBTL for test and evaluation.

Electrodes, cells and hardware components required to support development and test tasks will be fabricated.

4.4 PROGRAM MANAGEMENT

Program management will continue coordination of the development program and provide necessary program direction and control to enable achievement of overall performance objectives. Program management, quality assurance, and commercialization plans will be updated.

5.0 CONCLUSIONS

1. Fiber layups prepared by the needle-punching process, to reduce process costs by decreasing lay-up thickness and subsequently improving sintering furnace throughput, are now standard.

2. The Electroprecipitation process (EPP) nickel electrodes are delivering 24 Ah at target thickness (2.4 mm) and have demonstrated cyclic stability at 200+ test cycles.

3. Pasted nickel electrodes of 2.0 mm thickness have been fabricated which have demonstrated 23 Ah in full-size electrode tests and cyclic stability at 400+ test cycles to date.

4. Composite-type, full size iron electrodes have demonstrated 29 Ah at target thickness (1.0 mm). Cyclic stability has been demonstrated with electrodes at 1000+ cycles to date.

5. The separator system presently being used in the pilot line is Celanese K501/laminate, which enables cell resistance to be in the 0.70 to 0.80 m Ω range, an acceptable level to achieve the power density goal of >110 W/Kg.

6. Full-size nickel-iron cells have been constructed and tested that continue to demonstrate 57-61 Wh/Kg at the C/3 drain rate. Degradation in some of these cells seems to be related to nickel electrode swelling and subsequent stack electrolyte starvation during cycling.

7. A full-size cell has demonstrated cyclic stability with less than 20% degradation in capacity over 500 test cycles, with testing continuing.

8. A six cell module has demonstrated 327 cycles at NBTL. The capacity loss over this lifetime was approximately 26%.

9. Two batteries have been constructed in the pilot line facility for the DOE/JPL near-term electric vehicle program. These batteries are 25 Kwh at the C/3 rate. The first battery, with its auxiliary electrolyte/gas management system, is presently undergoing test and evaluation at JPL.

6.0 FY-1980 PUBLICATIONS AND PRESENTATIONS

1. "Fabrication of High Capacity Nickel Electrodes Using a Pasting Technique," J. Seidel/J. F. Jackovitz, Electrochemical Society, October 1979.

2. "Westinghouse Nickel Iron Battery Design and Performance," R. Rosey/B. E. Taber, EV EXPO '80, May 1980.

3. "An Advanced Technology Iron-Nickel Battery for Electric Vehicle Propulsion," W. Feduska/R. Rosey, Intersociety Energy Conversion Engineering Conference, August 1980.

4. "Annual Report for 1979 on Research, Development and Demonstration of Nickel Iron Batteries for Electric Vehicle Propulsion," Westinghouse Electric Corporation, R. Rosey et al, ANL/OEPM-79-14, June 1980.

7.0 ACKNOWLEDGEMENTS

The members of the program team who contributed to the work described in this report, and their major areas of responsibility are:

L. A. Doggrell - Separators, post-operation analyses of tested cells.

J. F. Jackovitz - Composite iron electrode, pasted nickel electrode, advanced concept cells.

C. W. Maiden - Electrical testing systems, module life test system design and construction.

N. J. Maskalick - EPP nickel electrode process development, advanced EPP concepts, cobalt substitution in the nickel active material, advanced concept cells.

W. Pollack - Electrode plaque process development, advanced plaque concepts.

L. G. Romain - EPP pilot line process, cell and module fabrication, formation line cell testing, cell and module testing.

J. Seidel - Composite iron electrode and process, pasted nickel electrode and process, advanced concept cells.

B. E. Taber - Component, cell, module and battery design, battery auxiliary systems design, battery testing, cell testing.

Members of the support team include:

D. R. Hart, Pilot Line Coordinator
A. Busofsky
J. H. Dugan
S. L. Karaffa
L. W. Martz
V. J. Mulvehill
E. A. Pantier
T. M. Valko
R. Wojcik

Distribution for ANL/OEPM-80-17

Internal:

J. J. Barghusen
D. Barney
M. H. Bhattacharyya
C. Bean
E. S. Beckjord
M. Bernard
E. C. Berrill
R. Biwer
A. Brown
L. Burris
G. Chapman
A. A. Chilenskas
C. C. Christianson
G. Cook
D. Corp
P. Cunningham
E. Creamer
S. A. Davis
W. DeLuca
R. C. Elliott
M. Farahat
P. R. Fields
F. Foster
D. Fredrickson
B. R. T. Frost
E. C. Gay
J. Geller
M. Genge
D. Graczyk
E. Hayes
L. Hill
F. Hornstra
C. C. Hsu
V. Kolba
J. Klinger
V. Kremesec
A. B. Krisciunas
M. Kronenberg
S. J. LaBelle
T. S. Lee
M. Liu
R. Loutfy
W. Massey
J. Meisenhelder
J. Miller
W. Miller
P. A. Nelson
M. V. Nevitt
E. G. Pewitt
D. Poa
J. Rajan
J. J. Roberts
M. F. Roche
H. Shimotake
R. K. Steunenberg
C. Swoboda
Z. Tomczuk
A. Tummillo
R. Varma
P. D. Vashishta
D. R. Vissers
D. S. Webster
F. Williams
F. Wyant
N. P. Yao (44)
ANL Contract File
ANL Libraries
TIS Files (6)

External:

DOE-TIC, for distribution per UC-94ca (318)
Manager, Chicago Operations and Regional Office, DOE
Chief, Office of Patent Counsel, DOE-CORO
V. Hummel, DOE-CORO
R. Gariboldi, DOE-CORO
Argonne Universities Association:
President
C. B. Alcock, U. of Toronto
W. L. Worrell, U. of Pennsylvania
W. Ahmad, KW Battery, Skokie, IL
R. Alkire, University of Illinois, Urbana
M. Allen, Mechanical Technology Inc., Latham, NY
E. T. Ames, TRW Systems, Redondo Beach, CA
L. Andrews, Electric Vehicle Council, Washington, DC
S. J. Angelovich, Mallory Battery Co., Tarrytown, NY
G. M. Arcand, Idaho State University, Pocatello
R. Aronson, Electric Field Propulsion Corp., Troy, MI
G. N. Ault, NASA Lewis Research Center
J. D. Baker, Stewart Warner Corp., Chicago
W. Bales, Jet Industries, Inc., Austin
H. Balzan, Chattanooga, TN
K. F. Barber, DOE, Office of Transportation Programs, Washington

T. Barber, Jet Propulsion Laboratory, Pasadena
R. J. Barkley, Compass Industries Inc., Hermosa Beach, CA
T. M. Barlow, Lawrence Livermore Laboratory
J. H. Hampton Barnett, Tennessee Valley Authority, Chattanooga
R. Barnstead, Aerospace Corporation, Washington DC
D. Barron, Delco-Remy Div., GMC, Anderson, IN
R. Bassett, Sandia Laboratory, Albuquerque
W. Bauer, Hittman Associates Inc., Columbia, MD
W. Bauer, KW Battery, Skokie, IL
E. Baumann, LILCO, Mineola, NY
W. C. Beasley, Union Carbide Corporation, New York, NY
H. Bell, Arizona Public Service Co., Phoenix
J. Bellack, Cleveland Electric Illuminating Co., Cleveland
L. Belove, Marathon Battery Corp., Waco, TX
W. R. Benn, Great Lakes Carbon Corporation, New York
D. Bennion, Brigham Young University, Provo, UT
C. Berger, Electrochemical & Water Desal. Technology, Santa Ana, CA
D. Bergmann, GM Transportation Systems Center, Warren, MI
L. Berkowitz, Esso Research Co., Linden, NJ
C. Berlsterling, C. Franklin Research Institute, Philadelphia
J. Birk, Electric Power Research Institute, Palo Alto
W. S. Bishop, Air Force Aero Propulsion Lab, Wright-Patterson AFB
D. P. Boden, C&D Batteries, Plymouth Meeting, PA
D. Borrello, Die Mesh Corporation, Pelham, NY
A. Borucka, Borucka Research Co., Livingston, NJ
P. Bowen, C&D Batteries, Plymouth Meeting, PA
D. Bowman, United States Postal Service, Washington
J. C. Boylan, Electric Dynamics Corp., Plainwell, MI
B. J. Bragg, Bell Laboratories, Murray Hill, NJ
J. Brennand, General Research Corp., Santa Barbara
A. F. Brewer, Malibu, CA
D. C. Briggs, Philco-Ford Corp., Palo Alto
P. Bro, P. R. Mallory & Co., Inc., Burlington, MA
J. Broadhead, Bell Laboratories, Murray Hill, NJ
E. P. Broglio, Eagle-Picher Industries, Joplin, MO
A. D. Brown, EVE Electric Motor Car, Inc., East Lansing, MI
P. J. Brown, DOE, Office of Transportation Programs, Washington
R. A. Brown, Eagle-Picher Industries, Joplin, MO
B. S. Brummer, EIC Corporation, Newton, MA
J. Bucci, C&D Batteries, Plymouth Meeting, PA
R. Buchholz, Honeywell Corp., Minneapolis
A. J. Burgess, Lucas Industries, Inc., Troy, MI
H. Burghart, Cleveland State University, Cleveland
D. Burns, Onan Corporation, Minneapolis
B. W. Burrows, Gould Inc., Rolling Meadows, IL
M. Burtgon, Delco-Remy Div. of GMC, Anderson, IN
J. D. Busi, USA Foreign Science & Tech. Center, Charlottesville, VA
E. Buzzelli, Westinghouse Electric Corp., Pittsburgh
W. P. Cadogan, Emhart Corp., Hartford, CT
E. Cairns, Lawrence Berkeley Lab.
E. Campbell, Electric Vehicle Consultants, Inc., New York, NY
P. Campbell, University of Southern California, Los Angeles
J. Campbell, DOT/UMTA, Washington, DC
R. T. Carpenter, Kimberly Clark Corp., Neenah, WI

T. V. Carvey, Hughes Aircraft Corp., Culver City, CA
A. Charkey, Energy Research Corp., Danbury, CT
L. D. Christian, General Electric, Gainesville
R. C. Chudacek, McGraw Edison Co., Bloomfield, NH
R. Clark, Sandia Labs., Albuquerque
J. E. Clifford, Battelle Memorial Institute, Columbus
J. A. Consiglio, Solva-Tek Associates, Topsfield, MA
A. R. Cook, ILZRO Inc., New York
K. E. Cooper, Trojan Battery Co., Santa Fe Springs, CA
G. Coraor, E. I. DePont de Nemours & Co., Inc., Wilmington, DE
R. E. Corbett, Lockheed Missiles & Space Co., Sunnyvale
D. Crane, United States Postal Service, Washington
R. A. Crawford, PPG Industries, Barberton, OH
C. Dacres, White Oak, Silver Spring, MD
R. H. Dare, Battronic Truck Corp., Boyertown, PA
D. Davis, Lawrence Livermore Laboratory
R. J. Dawson, Exide Management and Technology Co., Madison, WI
G. A. DeBari, INCO, Sterling Forest, Suffern, NY
J. Devitt, Denver, CO
A. N. Dey, P. R. Mallory & Co. Inc., Burlington, MA
W. J. Dippold, DOE, Office of Transportation Programs, Washington, DC
T. P. Dirske, Calvin College, Grand Rapids, MI
D. DiVirgillo, Lockheed Missiles and Space Co. Inc., Sunnyvale
D. Douglas, Electric Power Research Institute, Palo Alto
D. Dow, Detroit, MI
D. Dunoye, Reston, VA
T. Dwyer, Corning Glass Works, Corning, NY
E. F. Echolds, AiResearch Manufacturing Co., Torrance, CA
M. Eisenberg, Electrochimica Corp., Mountain View, CA
D. B. Eisenhaure, Charles Stark Draper Lab., Inc., Cambridge, MA
T. Eissenberg, Oak Ridge National Lab.
M. W. Ellison, Hughes Aircraft Corp., El Segundo
D. Elson, Black and Decker Inc., Towson, MD
C. English, University of New Mexico, Albuquerque
R. English, General Battery Co., Reading, PA
B. Enserik, Dynamic Science, Phoenix
R. Enters, McGraw Edison Co., Bloomfield, NJ
H. Espig, Gould Inc., Rolling Meadows, IL
E. C. Essig, Long Island Lighting Co., Mineola, NY
A. Ewing, DOE, Office of Transportation Program, Washington
G. Farbman, Westinghouse Electric Corp., Pittsburgh
D. W. Fedor, Bell Laboratories, Murray Hill, NJ
R. Fedora, Gould Inc., Rolling Meadows, IL
W. Feduska, Westinghouse Electric Corp., Pittsburgh
W. H. Fengler, Meteor Research Limited, Roseville, MI
F. Feres, KW Battery Co., Skokie, IL
R. Ferraro, Electric Power Research Institute
D. T. Ferrell, Exide Management and Technology Co., Yardley, PA
E. Fiss, Duke Power Co., Charlotte, NC
A. Fleischer, Orange, NJ
C. W. Fleischmann, C&D Batteries, Plymouth Meeting, PA
R. F. Fogle, North American Rockwell, Anaheim
R. T. Foley, American University, Washington, DC
F. Fontana, Consolidated Edison Co., Astoria, NY

L. R. Foote, Vehicle Systems Department, Ford Motor Co., Dearborn, MI
J. S. Fordyce, NASA Lewis Research Center
H. A. Fuggiti, Exide Management and Technology Co., Yardley, PA
T. Fujita, Pasadena, CA
B. Ganji, KW Battery Co., Skokie, IL
G. Gelb, Advanced Ground Systems, Long Beach, CA
J. H. B. George, George Consulting International Inc., Concord, MA
S. Geppert, Eaton Corporation, Southfield, MI
L. J. Gerlach, United States Postal Service, Rockville, MD
J. A. Gilchrist, Chloride America, Tampa
W. Gillespie, Structural Plastics Inc., Tulsa
J. R. Gilmore, Ford Motor Co., Dearborn, MI
C. Glassman, Transportation Research Center, East Liberty, OH
H. Glixon, Chevy Chase, MD
M. Globerman, General Services Administration, Washington
W. Goldman, Electric Vehicle Engineering, Lexington, MA
G. Goodman, Globe Battery Division, Milwaukee
R. E. Goodson, Purdue University
J. Gould, Unique Mobility Inc., Englewood, CO
L. B. Gratt, IWG Corp., San Diego
G. Greenberg, Electric Vehicle Battery Technology, Stamford, CT
H. Grepke, TurElec Inc., Bradenton, FL
D. Griter, Solar Centra, Mechanicsburg, OH
E. E. Grough, Lucas Industries Inc., Troy, MI
R. Guess, General Electric Research Lab., Schenectady
R. G. Gunther, General Motors Research Labs., Warren, MI
M. Hadden, Billing Energy Corp., Provo, UT
G. Hagey, DOE, Division of Technology Overview, Washington
H. Hamilton, University of Pittsburgh
W. Hamilton, General Research Corp., Santa Barbara
B. Hamlen, Exxon Enterprises Inc., Florham Park, NJ
D. Hanify, Fiat, Chicago
K. L. Hanson, General Electric Co., Philadelphia
W. Harhay, Electric Vehicle Associates, Cleveland
J. H. Harrison, Naval Ship R&D Center, Annapolis, MD
G. Hartman, Exide Management and Technology Co., Yardley, PA
J. Hartman, General Motors Research Labs., Warren, MI
C. Hayden, General Telephone and Electronics, Stamford, CT
E. A. Heintz, Airso Speer Carbon Graphite, Niagara Falls, NY
E. V. Hellman, Gould Inc., Langhorne, PA
R. Heppenstall, Penn Jersey Suburu Inc., Pennsauken, NJ
A. Himy, Naval Sea Systems Command, Washington
V. Hlavin, NASA Lewis Research Center
G. Hobbib, Exide Management and Technology Co., Cleveland
M. Hodgman, General Electric, Gainesville
R. Hoenburg, Mechanical Technology Inc., Latham, NY
R. Hudson, Eagle-Picher Industries, Joplin, MO
J. R. Huff, US Army Mobility Equipment R&D Command, Fort Belvoir, VA
H. L. Hughes, Oklahoma State University, Stillwater
W. Hull, USPS Research and Development Laboratory, Rockville, MD
B. Iseard, Freeport, Bahamas
H. R. Ivey, Wood-Ivey Systems Corp., Winter Park, FL
J. Jacus, Moore Haven, FL
M. A. Jansen, Allegheny Power Service Corporation, Greensburg, PA

G. H. Jantz, Rensselaer Polytechnic Institute
A. W. Johnson, General Electric Co., Philadelphia
L. Jokl, MERADCOM, Fort Belvoir, VA
K. R. Jones, Thiensville, WI
W. J. Jones, Westinghouse Electric Corp., Pittsburgh
R. E. Jordan, Omega Motors Corp., Garden Grove, CA
D. Kane, National Motors Corp., Lancaster, PA
E. Kanter, Gulton Battery Corp., Metuchen, NJ
N. Kaplan, Harry Diamond Laboratories, Washington
V. Kapur, Arco Solar Inc., Chatsworth, CA
R. Kaylor, Kaylor Energy Products, Menlo Park
J. Keith, Kaman Sciences, Colorado Springs, CO
J. J. Kelley, Exide Corporation, Yardley, PA
H. C. Kelly, OTA, U.S. Congress, Washington
J. G. Kennard, NASA Lewis Research Center
R. L. Kerr, Aero Propulsion Lab., Wright Patterson AFB
J. A. Kerrella, Delco-Remy Division/GMC, Anderson, IN
R. A. Keyes, Robert A. Keyes Associates, Martinsville, IN
R. A. Kingery, Oconomowoc, WI
R. S. Kirk, DOE, Office of Transportation Programs, Washington
M. Klein, Energy Research Corporation, Danbury, CT
G. B. Kliman, General Electric Co., Schenectady
G. B. Klinean, General Electric Co., Schenectady
R. C. Knechtli, Malibu, CA
R. A. Knight, AMF Inc., Stamford, CT
O. R. Kozak, American Battery Corp., Long Beach, NY
J. G. Krisilas, Aerospace Corporation, El Segundo, CA
P. E. Krouse, Exide Management & Technology Co., Yardley, PA
R. R. Kubalek, St. Joe Lead Co., Clayton, MD
L. Kulin, Whirlpool Corp. Benton Harbor, MI
C. M. Langkau, Union Carbide Co., Cleveland
H. Lauve, Electric Auto Corporation, Troy, MI
E. Lawlor, Membrana Incorporated, Chicago, IL
J. Lee, RAI Research Corp., Hauppauge, NY
I. J. Levine, Consolidated Edison, New York
K. Levine, St. Joe Minerals Corp., Pittsburgh
H. Lim, Hughes Research Lab., Malibu, CA
D. Linden, Little Silver, NJ
E. L. Littauer, Lockheed Palo Alto Research Laboratory
A. Long, Zeonics Corp., Fairfax, VA
E. Long, St. Joe Minerals Corp., Monaca, PA
P. Lu, Westinghouse Electric Corporation, Pittsburgh, PA
J. T. Lundquist, W. R. Grace & Co., Columbia, MD
T. Lynch, Fiber Materials, Inc., Biddeford, ME
E. N. Mabuce, Union Electric Co., St. Louis
J. MacDougall, AT&T, Basking Ridge, NJ
D. E. Mains, Naval Weapons Support Center, Crane, IN
J. Mader, Electric Power Research Institute, Palo Alto, CA
J. Maisel, Cleveland State University, Cleveland
J. S. Makulowich, Electric Vehicle Council, Washington
V. Manson, National Aeronautics and Space Adm., Washington
L. Mapa, KW Battery, Skokie, IL
L. S. Marcoux, Hughes Aircraft Company, Los Angeles
T. W. Martin, United States Postal Service, San Bruno, CA

J. Masson, Martin Marietta Corp., Denver, CO
C. E. May, NASA Lewis Research Center
E. Meeks, Derl Manufacturing Co., Compton, CA
J. D. Meiggs, Kaman Sciences Corp., Colorado Springs
P. Mighdoll, Booz-Allen & Hamilton, Cleveland
R. P. Mikkelson, General Dynamics, San Diego
D. G. Miley, U.S. Naval Ammunition Depot, Crane, IN
H. Miller, Department of Transportation, Cambridge, MA
D. K. Miner, Copper Development Associates, Birmingham, MD
L. G. Morin, Tarrytown, NY
F. Morse, Silver Spring, MD
A. Moss, Leesona Moos Laboratories, Warwick, RI
R. Mueller, University of California, Berkeley
J. H. Muir, Dimension V Inc., Indialantic, FL
J. P. Mullin, National Aeronautics & Space Administration, Washington
G. Murphy, Northwestern University
N. T. Musial, Nasa Lewis Research Center
B. McCormick, Los Alamos Scientific Lab.
L. R. McCoy, Energy Systems Group, Canoga Park
A. H. McCutcheon, Texas State University, Waco, TX
R. McKee, McKee Engineering, Palatine, IL
F. McLarnon, Lawrence Berkeley Lab.
J. N. McNamara, Northrup Corporation, Hawthorne, CA
P. McRay, ILC Technology, Sunnyvale
W. J. Nagle, NASA Lewis Research Center
L. Nalley, Creative Research Co., Roebuck, SC
J. Newman, Univ. of California, Berkeley
J. S. Newton, Newton Engineering Co., Glen Ellyn, IL
A. O. Nilsson, NIFE Incorporated, Lincoln, RI
J. Norberg, Exide Management & Technology Co., Philadelphia
A. C. Occhipinti, Kenner, LA
L. G. O'Connell, Lawrence Livermore Lab.
G. Odom, Georgia Power Company, Atlanta, GA
R. Oglesby, GM Transportation Systems Ctr., Warren, MI
L. Omohundro, Kingery Research & Development, Wake Forest, NC
E. I. Onstott, Los Alamos Scientific Lab
R. Osteryoung, State University of New York at Buffalo
B. N. Otzinger, North American Aviation, Downey, CA
J. P. Overman, Hammond Lead Products Inc., Hammond, IN
J. E. Oxley, Gould Inc., Rolling Meadows, IL
E. Papandreas, REI, Lake Worth, FL
J. S. Parkinson, Johns-Manville R&D Center, Manville, NJ
J. M. Parry, Arthur D. Little Inc., Cambridge, MA
E. Patagalia, General Services Administration, Washington
S. Pauling, Naperville, IL
J. E. Pavolsky, NASA/Lyndon B. Johnson Space Ctr., Houston
C. Pax, DOE, Office of Transportation Programs, Washington
E. Pearlman, Exide Management and Technology Co., Yardley, PA
J. P. Pemsler, Castle Technology Corp., Lexington, MA
G. F. Pezdirtz, DOE, Office of Advanced Conservation Technology, Washington
A. Pivec, Public Service Electric and Gas, Newark, NJ
A. G. Plunckett, General Electric R&D Center, Schenectady
R. A. Powers, Union Carbide Corp., Cleveland
V. J. Puglisi, Yardney Electric Corp., Pawcatuck, CT

E. Ramirez, Amectran, Dallas
A. D. Raynard, AiResearch Manufacturing Co., Torrance, CA
E. C. Read, Exxon Enterprises, Linden, NJ
H. L. Recht, Atomics International Division, Canoga Park
C. Ridgway, Walt Disney World Co., Lake Buena Vista, FL
W. Rippel, Jet Propulsion Laboratory, Pasadena
E. Rizkalla, DOE, Office of Controller, Washington
R. A. Rizzo, Globe Battery Division, Milwaukee
R. Robert, The MITRE Corporation, McLean, VA
F. T. Rooney, Bureau of Automotive Maintenance, Norfolk, VA
L. Rosenblum, NASA Lewis Research Center
N. Rosenburg, Department of Transportation, Cambridge, MA
R. Rosey, Westinghouse, Pittsburgh
J. Rossmon, Cornell University
G. Rowland, General Electric, Schenectady
J. Rubenzer, NASA Ames Research Center, Moffett Field
P. H. Rubie, Electric Passenger Cars, Inc., San Diego
H. E. Ruskie, Naval Intelligence Support Center, Washington
A. J. Salkind, Rutger Medical School, Piscataway, NJ
R. T. Schneider, RTS Laboratories, Gainesville, FL
L. W. Schopen, NASA Lewis Research Center
H. J. Schwartz, NASA Lewis Research Center
W. R. Scott, TRW Systems Inc., Redondo Beach
H. Seigel, South Coast Technology Inc., Santa Barbara, CA
H. Seiger, Harvey Seiger Associates, Waterford, CT
J. Seliber, Fluid Drive Engineering Co., Wilmette, IL
E. Seo, Gates Energy Products, Denver, CO
L. Shahnasarian, Elcar Corp., Elkhart, IN
R. C. Shair, CENTREC Corporation, Fort Lauderdale
H. Shalit, ARCO Chemical Corp., Glendolden, PA
D. W. Sheibley, NASA Lewis Research Center
G. L. Silverman, Ford Motor Co., Dearborn, MI
E. Small, Amectran Corporation, Washington
G. A. Smith, Englehard Industries, Iselin, NJ
S. Smith, St. Joe Minerals Corp., Monaca, PA
V. Smith, Delco-Remy Div. GMC, Anderson, IN
J. Smits, Nevada Operations Office, Las Vegas
I. J. Soloman, IIT Research Institute, Chicago
W. C. Spindler, Electric Power Research Institute, Palo Alto
J. S. Stanley, U.S. Army Foreign Sci. & Tech. Center, Charlottesville, VA
E. J. Steeve, Commonwealth Edison Co., Chicago
I. Stein, Jet Propulsion Laboratory, Pasadena
T. A. Stoneham, Marathon Battery Company, Waco, TX
R. Strauss, Communications Satellite Corp., Clarksburg, MD
W. E. Strawbridge, Caterpiller Tractor Co., Peoria, IL
R. L. Strombotne, DOE, Department of Transportation, Washington, DC
S. Sudar, Rockwell International, Canoga Park
P. C. Symons, Birmingham, MI
F. Tepper, Catalyst Research Corp., Baltimore
R. Thacker, General Motors Research Labs, Warren, MI
C. E. Thomas, Chrysler Corporation, New Orleans, LA
F. Thomas, Grumman Aerospace Corp., Bethpage, NY
M. Thorpe, Towson, MD
G. M. Thur, DOE, Office of Transportation Programs, Washington

W. H. Tiedemann, Globe Battery Division, Milwaukee
C. W. Tobias, University of California, Berkeley
A. Topouzian, Ford Motor Co., Dearborn, MI
W. Toth, Society of Automotive Engineers, Inc., Warrendale, PA
H. Toulmin, Bloomfield, MI
I. Trachtenberg, Texas Instruments, Dallas
J. C. Trocciola, United Technologies Corp., South Windsor, CT
G. W. Tuffnell, The International Nickel Co., Troy, MI
D. Turford, Western Mining Corp., Pittsburgh
G. H. Turney, Western Research Industries, Las Vegas, NV
E. A. Ulrich, Creative Automotive Research, Whittier, CA
R. L. Ulrich, General Services Administration, Washington
T. Ulrich, McGraw-Edison Co., Bloomfield, NJ
G. Underhill, A. D. Little, Cambridge, MA
H. B. Urbach, Naval Ship R&D Center, Annapolis, MD
H. Vaidyanathan, Energy Research Corp., Danbury, CT
C. J. Venuto, C&D Batteries, Plymouth Meeting, PA
S. W. Vreeland, General Dynamics, Convair Division, San Diego
A. Waddell, EBCO Battery Co., Columbus, GA
E. H. Wakefield, Linear Alpha Inc., Evanston, IL
R. Walker, University of Florida, Gainesville
C. H. Waterman, C. H. Waterman Industries, Althol, MA
G. Way, Troy, MI
W. Webster, DOE, Office of Advanced Conservation Technology, Washington
R. D. Wehrle, Sandia Labs, Albuquerque, NM
S. A. Weiner, Ford Motor Co., Detroit, MI
C. Weinlein, Globe Battery Division, Milwaukee
M. Weinreb, Con Edison, New York
E. Y. Weissman, GASF Wyandotte Corp., Wyandotte, MI
I. Wender, Bureau of Mines, Pittsburgh, PA
H. B. West, McGraw-Edison Company, Bloomfield, NJ
J. H. Whitmore, Binghamton, NY
M. E. Wilke, Burgess Battery Company, Freeport, IL
R. Wilks, Lavelle Aircraft Co., Newton, PA
C. F. Williams, Teledyne Isotopes, Timonium, MD
H. R. Williams, Detroit Edison Co., Detroit
J. M. Williams, E. I. duPont de Nemours & Co., Wilmington, DE
E. Willhnganz, C&D Batteries, Plymouth Meeting, PA
N. L. Willmann, Delco Remy Div. of GMC, Anderson, IN
J. F. Wing, Booz-Allen & Hamilton Inc., Bethesda, MD
G. A. Wooldrige, Boeing Aerospace Co., Seattle
V. Wouk, Petro-Electric Motor Ltd., New York
R. A. Wynveen, Life Systems Inc., Cleveland
L. Yanni, Booz-Allen and Hamilton, Bethesda, MD
L. S. Yao, University of Illinois, Urbana
H. Yoder, Battronic Truck Corp., Boyertown, PA
M. Yontar, Jersey City, NJ
R. Zalosh, Factory Mutual Research, Norwood, MA
J. E. Zanks, NASA Langley Research Center, Hampton, VA
M. Zlotnick, Divison of Conservation Research and Technology, Washington, DC